Macromolecules

pubs.acs.org/Macromolecules Article

Theory of Microphase Separation in Concentrated Solutions of Sequence-Specific Charged Heteropolymers

Siao-Fong Li and Murugappan Muthukumar*

Cite This: *Macromolecules* 2022, 55, 5535−5549 Read Online

ACCESS | Metrics & More | Article Recommendations | Supporting Information

ABSTRACT: We present a general theory of the phase behavior of concentrated multicomponent solutions of charged flexible heteropolymers with specific chemical sequences. Using a field theoretic formalism, we have accounted for sequence specificity, electrostatic and van der Waals interactions among all constituent species, and topological correlations among all heteropolymer chains in the system. Our general expression for the Helmholtz free energy of the system is in terms of density profiles of the various components and is an explicit function of the sequence specificity of the heteropolymers, polymer concentration, salt concentration, chemical mismatch among the various monomers and solvent, and temperature. We illustrate our general theory in the context of the self-assembly of intrinsically disordered proteins by considering solutions of sequence-specific charged-neutral heteropolymers. For the heteropolymers under consideration, the system exhibits microphase separation. The boundaries of order−disorder transition and the relative stabilities of the canonical microphase-separated morphologies (lamellar, cylindrical, and spherical) are presented in the weak segregation limit as functions of sequence, polymer concentration, chemical mismatch parameters, and salt concentration. Unique mapping between heteropolymer sequence and morphology diagram is presented. The derived general theory is of broad applicability in addressing sequence effects on the thermodynamic behavior of any multicomponent system containing flexible heteropolymers.

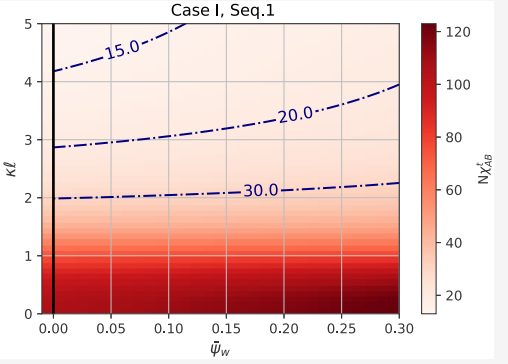

1. INTRODUCTION

While the theory of the phase behavior of solutions of homopolymers and block copolymers is at an advanced stage capable of quantitative predictions on macrophase and microphase separation phenomena, the formulation of a general theory for multicomponent heteropolymers with sequence specificity continues to be a challenge. The imminent need for addressing this challenge is instigated by the prolific emergence of biomolecular condensates (also known as membraneless organelles) formed by intrinsically disordered proteins (IDPs)[1] and synthetic polypeptoids.[2,3] It is well-known that the structures of folded proteins are uniquely determined by their sequences of the amino acid units constituting the protein molecule.[4] However, in the case of IDPs, the sequence−structure relationship is only at early stages of understanding. The main feature of IDPs is their sequence-driven intrinsic capacity for extensive conformational fluctuations arising from optimization between electrostatic and hydrophobic interactions. In the context of dilute solutions of IDPs, there are a few excellent theories and simulations of isolated IDP molecules that demonstrate the significant role of sequences on molecular conformations.[5−11] However, in the context of biomolecular condensates, the self-assembly process involves many IDP molecules with specific sequences and several components. It is this ubiquitous premise where we present a general theory of sequence effects on the self-assembly of concentrated solutions of heteropolymers by accounting for topological and electrostatic correlations and hydrophobicity effects. A cursory inspection of amino acid sequences of typical IDPs suggests the presence of multi-domains of charged, dipolar, and uncharged[12] repeat units with varying frequencies along their chain backbone. It is well-known that, in the other extreme situation of synthetic polymers without any charges, diblock copolymers exhibit the phenomenon of microphase separation with the emergence of several well-organized stable morphologies depending on the composition and length of the diblock copolymer and the temperature.[13−38] Therefore, it is natural to raise the issue of microphase separation in solutions of IDPs too. By following the footsteps of the previous theories[36,39,40] of microphase separation of uncharged or charged diblock copolymer systems, there have been only a few attempts to address simple specific sequences with limited success.[41,42] Further-

Received: January 3, 2022
Revised: June 6, 2022
Published: June 27, 2022

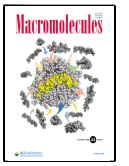

https://doi.org/10.1021/acs.macromol.2c00008
Macromolecules 2022, 55, 5535−5549

more, there have also been simulation studies to explore the sequence effects for a few specific sequences.[3,43−45]

In this paper, we present a general theory of concentrated solutions of multicomponent heteropolymers made up of any number of different kinds of monomers and any kinds of intermonomer and monomer−solvent interactions (such as electrostatic, dipolar, and short-ranged van der Waals). Starting from the Edwards Hamiltonian that models the chain connectivity, monomer sequence, and all interspecies interactions, we have derived the Helmholtz free energy as a functional of the density profiles of the various components of the system. An approximate expression for the free energy is evaluated using the saddle point approximation. It not only is consistent with previous random phase approximation (RPA) results but also is able to predict the length scales of microphase separation based on the sequence scales[41] of sequences explicitly and properly without introducing any additional parameters. Even in the homogeneous phase, the system can exhibit preferred structures of well-defined microscopic length scales, a feature that is the earmark of microphase separation. However, it can be destroyed by increasing the amount of solvent. Under such conditions, the system can show only macrophase separation, commonly referred to as the liquid−liquid phase separation (LLPS). An interference between them enriches the phase behaviors,[46] but we will focus on the microphase separation in the paper. While the derived free energy expression is valid for all extents of segregation, in this paper we have focused on the limit of weak segregation when microphase separation occurs and have computed the boundaries of disorder−order and the various order−order transitions. We illustrate the consequences of this general theory with the example of sequence effects on microphase separation in solutions of two-component (charge and neutral) heteropolymers, an approximation of amino acids,[43−45] by focusing on the limit of weak segregation. For the sake of simplicity in our simple model, we treat the charged monomers as test charges. Following our earlier work,[47−50] we integrate the degrees of freedom of counterions and salt ions and obtain the contribution from the translational entropy of dissociated ions and also derive the Debye−Hückel (DH) interaction,[47−49,51] which is free from any artificial mathematical divergences. Furthermore, since we treat only the weak segregation limit in the present study, we have taken the distribution of small ions to be uniform as suggested by the results from RPA.[40,52]

The results described below show the significant role played by chemical sequences in the microphase-separated morphology diagrams of multicomponent heteropolymers. More significantly, the derived theory provides a computational engine to address the microphase separation behavior of concentrated solutions of flexible heteropolymers with an arbitrary number of different kinds of monomers in the presence of added salt.

The outline of the rest of the paper is as follows. The theoretical model and formalism for the illustrative example of solutions of two-component (charge-neutral) heteropolymers are introduced in Section 2. The computed results are presented in Section 3. The final section summarizes the main conclusions on the sequence effects for the illustrative example. Owing to the mathematical richness of the formalism, details of the general theory are presented in the Supporting Information.

2. MODEL AND THEORY

Let us consider a solution of n_p flexible heteropolymer chains, each of N repeat units made up of $\mathbb{M}$ kinds of repeat units and $\mathbb{m}$ kinds of small molecules or ions, each with n_{ws} $(1 \le s \le \mathbb{m})$ number. The total volume of the system is Ωl^3, where l is the unit of length. For the sake of avoiding too many labels for the nonuniversal microscopic sizes of different repeat units, solvent molecules, and dissociated ions, we take l as the average size of each of these species. All potential interactions among the various species including electrostatic and short-ranged excluded volume interactions are denoted by U. The partition function for this general scenario is given in the Supporting Information. In order to make this general theory more transparent in terms of the used assumptions and approximations, we illustrate the theory for a simpler system.

In the simple system, there are n_p two-component heteropolymer chains of N Kuhn segments, each of segment length l. Each chain contains $N_A = N/2$ neutral A segments and $N_B = N/2$ charged B segments arranged in specified sequences. The charge on the B segments is of the same sign as the value of $z_p e$ (where e is the electronic charge). There is only one solvent in the system with n_w as the number of the solvent molecules. The dissociated ions n_γ from the heteropolymer and added salt are treated implicitly as an electrolyte continuum, described by the linearized Debye−Hückel theory although the electrolyte continuum is non-neutral.[48] The electrostatic interaction between two charged (B) segments with the separation distance r is given by the Debye−Hückel potential[47] energy v_{el}

$$v_{el}(r) = \frac{z_p^2 l_B}{r} e^{-\kappa r} \tag{1}$$

$$\mathcal{Z}_{plasma} = \exp\left(-\sum_\gamma n_\gamma \ln\left(\frac{n_\gamma}{\Omega}\right) + \Omega\frac{\kappa^3 l^3}{12}\right) \tag{2}$$

where l_B is the Bjerrum length $(e^2/4\pi\epsilon\epsilon_0 k_B T$, where ϵ_0 is the vacuum permittivity, ϵ is the dielectric constant of the solvent, and $k_B T$ is the Boltzmann constant times the absolute temperature), and κ is the inverse Debye length.[53] $\mathcal{Z}_{plasma}$ is the partition function due to the entropy of ions $n_\gamma \ln\left(\frac{n_\gamma}{\Omega}\right)$ and fluctuations of ions $\Omega\frac{\kappa^3 l^3}{12}$, and $-k_B T \ln \mathcal{Z}_{plasma}$ is the Helmholtz free energy F_{plasma} from the background fluid. In addition, the short-ranged van der Waals interactions between the various segments (A and B) of the heteropolymer and solvent molecule (w) are represented by delta functions with strength given by the excluded volume parameters v_{AA}, v_{BB}, v_{ww}, v_{AB}, v_{Aw}, and v_{Bw}. Furthermore, we assume that the system is incompressible.

The additional contribution from the interacting polymer chains to the Helmholtz free energy F of the system is given by $-k_B T \ln \mathcal{Z}$, where the partition function $\mathcal{Z}$ is modeled through the generalized Edwards Hamiltonian as

https://doi.org/10.1021/acs.macromol.2c00008
Macromolecules 2022, 55, 5535−5549

$$\mathcal{Z} = \frac{1}{n_p! n_w!} \int \prod_{j=1}^{n_w} \mathrm{d}\vec{r}_j \prod_{\alpha=1}^{n_p} \mathcal{D}\{\vec{R}_\alpha(s)\} \times \exp\left[-\frac{3}{2l^2}\sum_{\alpha=1}^{n_p}\int_0^N \mathrm{d}s\left(\frac{\partial \vec{R}_\alpha(s)}{\partial s}\right)^2 - \frac{U}{k_B T}\right] \times \prod_{\vec{r}} \delta\left[l^3 \sum_{j=1}^{n_w} \delta(\vec{r} - \vec{r}_j) + l^3 \sum_{\alpha=1}^{n_p}\int_0^N \mathrm{d}s \delta(\vec{r} - \vec{R}_\alpha(s)) - 1\right] \tag{3}$$

Here $\vec{r}_j$ is the position vector of jth solvent molecule, $\vec{R}_\alpha(s)$ is the position vector of the αth chain contour at the arc length location of the sth segment, and the functional integral over $\mathcal{D}\{\vec{R}_\alpha(s)\}$ is the sum over all allowed chain conformations including integration over positions of chain ends. The first term inside the argument of the exponential depicts the chain connectivity, and U is the potential interaction energy as given below. The factor of the product over $\vec{r}$ corresponds to the incompressibility constraint.

As mentioned above, U denotes all two-body interactions parametrized by v_{AA}, v_{BB}, v_{ww}, v_{AB}, v_{Aw}, and v_{Bw} as

$$\begin{aligned}\frac{U}{k_B T} = {} & \frac{1}{2}\sum_{\alpha=1}^{n_p}\int_0^N \mathrm{d}s \sum_{\alpha'=1}^{n_p}\int_0^N \mathrm{d}s' \sigma_A(s)\sigma_A(s') v_{AA} l^3 \times \delta(\vec{R}_\alpha(s) - \vec{R}_{\alpha'}(s')) + \frac{1}{2}\sum_{\alpha=1}^{n_p}\int_0^N \mathrm{d}s \\ & \sum_{\alpha'=1}^{n_p}\int_0^N \mathrm{d}s' \sigma_B(s)\sigma_B(s') v_{BB} l^3 \delta(\vec{R}_\alpha(s) - \vec{R}_{\alpha'}(s')) \\ & + \frac{1}{2}\sum_{\alpha=1}^{n_p}\int_0^N \mathrm{d}s \sum_{\alpha'=1}^{n_p}\int_0^N \mathrm{d}s' \sigma_B(s)\sigma_B(s') \\ & v_{el}(|\vec{R}_\alpha(s) - \vec{R}_{\alpha'}(s')|) + \sum_{\alpha=1}^{n_p}\int_0^N \mathrm{d}s \\ & \sum_{\alpha'=1}^{n_p}\int_0^N \mathrm{d}s' \sigma_A(s)\sigma_B(s') v_{AB} l^3 \delta(\vec{R}_\alpha(s) - \vec{R}_{\alpha'}(s')) \\ & + \sum_{\alpha=1}^{n_p}\int_0^N \mathrm{d}s \sum_{j=1}^{n_w} [\sigma_A(s) v_{Aw} l^3 + \sigma_B(s) v_{Bw} l^3] \\ & \delta(\vec{R}_\alpha(s) - \vec{r}_j) + \frac{1}{2}\sum_{j=1}^{n_w}\sum_{j'=1}^{n_w} v_{ww} l^3 \delta(\vec{r}_j - \vec{r}_{j'})\end{aligned} \tag{4}$$

where the variable $\sigma_{A(B)}(s)$ denotes the sequence of the heteropolymer

$$\sigma_{A(B)}(s) = \begin{cases} 1, & \text{if the } s\text{th segment is A(B)} \\ 0, & \text{otherwise} \end{cases} \tag{5}$$

and v_{el} in the third term on the right-hand side is given by eq 1.

Introducing the microscopic variables

$$\begin{aligned}\hat{\psi}_w(\vec{r}) &= l^3 \sum_{j=1}^{n_w} \delta(\vec{r} - \vec{r}_j) \\ \hat{\psi}_{A(B)}(\vec{r}) &= l^3 \sum_{\alpha=1}^{n_p}\int_0^N \mathrm{d}s \sigma_{A(B)}(s)\delta(\vec{r} - \vec{R}_\alpha(s))\end{aligned} \tag{6}$$

the partition function becomes

$$\mathcal{Z} = \frac{1}{n_p! n_w!} \int \prod_{j=1}^{n_w} \mathrm{d}\vec{r}_j \prod_{\alpha=1}^{n_p} \mathcal{D}\{\vec{R}_\alpha(s)\} \times \exp\left[-\frac{3}{2l^2}\sum_{\alpha=1}^{n_p}\int_0^N \mathrm{d}s\left(\frac{\partial \vec{R}_\alpha(s)}{\partial s}\right)^2 - \frac{U}{k_B T}\right] \times \prod_{\vec{r}} \delta[\hat{\psi}_w(\vec{r}) + \hat{\psi}_A(\vec{r}) + \hat{\psi}_B(\vec{r}) - 1] \tag{7}$$

where

$$\begin{aligned}\frac{U}{k_B T} = {} & \frac{U_0}{k_B T} + \int \frac{\mathrm{d}\vec{r}}{l^3}[\hat{\psi}_A(\vec{r})(\chi_{Aw} l^3)\hat{\psi}_w(\vec{r}) + \\ & \hat{\psi}_B(\vec{r})(\chi_{Bw} l^3)\hat{\psi}_w(\vec{r}) + \hat{\psi}_A(\vec{r})(\chi_{AB} l^3)\hat{\psi}_B(\vec{r})] \\ & + \frac{1}{2}\int \frac{\mathrm{d}\vec{r}}{l^3}\frac{\mathrm{d}\vec{r}'}{l^3}\hat{\psi}_B(\vec{r})\left(\frac{z_p^2 l_B}{|\vec{r} - \vec{r}'|} e^{-\kappa|\vec{r} - \vec{r}'|}\right)\hat{\psi}_B(\vec{r}')\end{aligned} \tag{8}$$

where χ_{ij} are the Flory–Huggins parameters given as

$$\chi_{ij} = v_{ij} - \frac{v_{ii} + v_{jj}}{2} \tag{9}$$

with i and j denoting A, B, and w. The constant term $U_0/k_B T$ is $(v_{AA} n_p N_A + v_{BB} n_p N_B + v_{ww} n_w)/2$, which does not have any consequence on the derivatives of the free energy of the system. Equation 7 is the starting point for the illustrative simple model for further theoretical analysis. The l will not be written down explicitly in the following sections.

The partition function $\mathcal{Z}$ in eq 7 is in terms of microscopic variables, and all chains are coupled through interactions among all species in the system. As the next step, we rewrite $\mathcal{Z}$ in terms of macroscopic density fields which are experimentally measurable and also decouple the chains using these fields.

2.1. Coarse-Grained Partition Function. Introducing the microscopic density fields $\psi(\vec{r})$ for each of the microscopic variables $\hat{\psi}(\vec{r})$ and using the identity

$$\begin{aligned}1 &= \int \mathcal{D}\{\psi(\vec{r})\} \prod_{\vec{r}} \delta[\psi(\vec{r}) - \hat{\psi}(\vec{r})] \\ &= \int \mathcal{D}\{\psi(\vec{r})\}\mathcal{D}\{\mu(\vec{r})\} \exp\left[i \int \mathrm{d}\vec{r}\mu(\vec{r})(\psi(r) - \hat{\psi}(r))\right]\end{aligned} \tag{10}$$

eq 7 becomes

https://doi.org/10.1021/acs.macromol.2c00008
Macromolecules 2022, 55, 5535−5549

$$\mathcal{Z} = \int \mathcal{D}\{\psi_w(\vec{r})\}\mathcal{D}\{\psi_A(\vec{r})\}\mathcal{D}\{\psi_B(\vec{r})\} \prod_{\vec{r}} \delta[\psi_w(\vec{r}) + \psi_A(\vec{r}) + \psi_B(\vec{r}) - 1] \exp\left[-\frac{U}{k_BT}(\{\psi_w\}, \{\psi_A\}, \{\psi_B\})\right] \times \int \mathcal{D}\{\mu_w(\vec{r})\} \exp\left[i\int d\vec{r}\mu_w(\vec{r})\psi_w(\vec{r})\right]\frac{1}{n_w!} \int\prod_{j=1}^{n_w} d\vec{r}_j \exp\left[-i\int d\vec{r}\mu_w(\vec{r})\hat{\psi}_w(\vec{r})\right] \times \int \mathcal{D}\{\mu_A(\vec{r})\}\mathcal{D}\{\mu_B(\vec{r})\}\exp\left[i\int d\vec{r}(\mu_A(\vec{r})\psi_A(\vec{r}) + \mu_B(\vec{r})\psi_B(\vec{r}))\right] \times \frac{1}{n_p!}\int\prod_{\alpha=1}^{n_p}\mathcal{D}\{\vec{R}_\alpha(s)\} \exp\left[-\frac{3}{2l^2}\sum_\alpha\int ds\left(\frac{\partial\vec{R}_\alpha(s)}{\partial s}\right)^2 - i\int d\vec{r}(\mu_A(\vec{r})\hat{\psi}_A(\vec{r}) + \mu_B(\vec{r})\hat{\psi}_B(\vec{r}))\right] \tag{11}$$

where $U(\{\psi_w\}, \{\psi_A\}, \{\psi_B\})$ means that the microscopic variables $\hat{\psi}$ in eq 8 are replaced by the macroscopic ψ.

2.2. Coarse-Grained Partition Function in Terms of Fourier Components. The partition function can be separated into two parts. One is the mean field contribution, and the other arises from fluctuations. In order to facilitate extraction of the mean field part, we define the Fourier transform of $\psi(\vec{r})$ as

$$\psi(\vec{q}) = \int d\vec{r}\psi(\vec{r})e^{i\vec{q}\cdot\vec{r}} \tag{12}$$

Using this definition, $\mathcal{Z}$ can be separated into mean field and fluctuations contributions as

$$\mathcal{Z} = \int \mathcal{D}\{\psi_w(0)\}\mathcal{D}\{\psi_A(0)\}\mathcal{D}\{\psi_B(0)\} \delta[\psi_w(0) + \psi_A(0) + \psi_B(0) - \Omega] \times \delta[\psi_w(0) - \Omega\overline{\psi}_w]\delta[\psi_A(0) - \Omega\overline{\psi}_A]\delta[\psi_B(0) - \Omega\overline{\psi}_B] \times \int_{\vec{q}\neq 0}\mathcal{D}\{\psi_w(\vec{q})\}\mathcal{D}\{\psi_A(\vec{q})\}\mathcal{D}\{\psi_B(\vec{q})\} \prod_{\vec{q}\neq 0}\delta[\psi_w(\vec{q}) + \psi_A(\vec{q}) + \psi_B(\vec{q})]\exp -\frac{U}{k_BT} \times \int_{\vec{q}\neq 0}\mathcal{D}\{\mu_w(\vec{q})\}\exp\left[i\int_{\vec{q}\neq 0}\frac{d\vec{q}}{(2\pi)^3}\mu_w(\vec{q})\psi_w(-\vec{q}) - \frac{H_w}{k_BT}\right] \times \int_{\vec{q}\neq 0}\mathcal{D}\{\mu_A(\vec{q})\}\mathcal{D}\{\mu_B(\vec{q})\} \exp\left[i\int_{\vec{q}\neq 0}\frac{d\vec{q}}{(2\pi)^3}(\mu_A(\vec{q})\psi_A(-\vec{q}) + \mu_B(\vec{q})\psi_B(-\vec{q})) - \frac{H_p}{k_BT}\right] \tag{13}$$

where $\psi(0)$ denotes the mean field $\psi(\vec{q} = 0)$, $\overline{\psi}_w = n_w/\Omega$, $\overline{\psi}_{A(B)} = N/2 \times n_p/\Omega$, and $H_w/k_BT(\{\mu_w\})$ and $H_p/k_BT(\{\mu_A\}, \{\mu_B\})$ are related to the integrals over position vectors

$$\frac{H_w}{k_BT} = \ln n_w! - \ln\left\{\int\prod_{j=1}^{n_w} d\vec{r}_j \exp\left[-i\int_{\vec{q}\neq 0}\frac{d\vec{q}}{(2\pi)^3}\mu_w(\vec{q})\hat{\psi}_w(-\vec{q})\right]\right\} = \ln n_w! - n_w\ln\left\{\int d\vec{r}\exp\left[-i\int_{\vec{q}\neq 0}\frac{d\vec{q}}{(2\pi)^3}\mu_w(\vec{q})e^{i\vec{q}\cdot\vec{r}}\right]\right\} \tag{14}$$

$$\frac{H_p}{k_BT} = \ln n_p! - \ln\left\{\int\prod_{\alpha=1}^{n_p}\mathcal{D}\{\vec{R}_\alpha(s)\}\exp\left[-\frac{3}{2l^2}\sum_\alpha\int ds\left(\frac{\partial\vec{R}_\alpha(s)}{\partial s}\right)^2 - i\int_{\vec{q}\neq 0}\frac{d\vec{q}}{(2\pi)^3}(\mu_A(\vec{q})\hat{\psi}_A(-\vec{q}) + \mu_B(\vec{q})\hat{\psi}_B(-\vec{q}))\right]\right\} = \ln n_p! - n_p\ln\left\{\int\mathcal{D}\{\vec{R}(s)\}\exp\left[-\frac{3}{2l^2}\int ds\left(\frac{\partial\vec{R}(s)}{\partial s}\right)^2 - i\int_{\vec{q}\neq 0}\frac{d\vec{q}}{(2\pi)^3}\int ds(\mu_A(\vec{q})\sigma_A(s) + \mu_B(\vec{q})\sigma_B(s))e^{i\vec{q}\cdot\vec{R}(s)}\right]\right\} \tag{15}$$

The second rows of eq 14 and eq 15 are due to the decoupling of the solvent molecules and chains, respectively, arising from the introduction of the density fields. Since there is no explicit integral for H_w/k_BT and H_p/k_BT, it is necessary to expand them as asymptotic series, as derived in the following subsection. Complementary to this procedure, we can also derive an approximate free energy based on self-consistent field theoretic formulation as given in the Supporting Information.

2.3. Series Expansions of H_w/k_BT and H_p/k_BT. The asymptotic series with respect to $\mu_w(\vec{q}) = 0$ and $\mu_{A(B)}(\vec{q}) = 0$ are given as

$$\frac{H_w}{k_BT} = (\ln n_w! - n_w\ln\Omega) - \sum_{n=1}\frac{(-i)^n}{n!}\int_{\vec{q}\neq 0}\frac{d\vec{q}_1}{(2\pi)^3}, ..., \frac{d\vec{q}_n}{(2\pi)^3}\mathbb{G}^{(n)}_{w,...,w}(\vec{q}_1, ..., \vec{q}_n)\overbrace{\mu_w(\vec{q}_1), ..., \mu_w(\vec{q}_n)}^{n} \tag{16}$$

$$\frac{H_p}{k_BT} = (\ln n_p! - n_p\ln\Omega) - \sum_{n=1}\frac{(-i)^n}{n!}\sum_{i1=\{A,B\}}, ..., \sum_{in=\{A,B\}}\int_{\vec{q}\neq 0}\frac{d\vec{q}_1}{(2\pi)^3}, ..., \frac{d\vec{q}_n}{(2\pi)^3}\mathbb{G}^{(n)}_{i1,...,in}(\vec{q}_1, ..., \vec{q}_n)\mu_{i1}(\vec{q}_1), ..., \mu_{in}(\vec{q}_n) \tag{17}$$

where the $\mathbb{G}^{(n)}$ are given by

https://doi.org/10.1021/acs.macromol.2c00008
Macromolecules 2022, 55, 5535−5549

$$\mathbb{G}^{(n)}_{\mathrm{w},\ldots,\mathrm{w}}(\vec{q}_1, \ldots, \vec{q}_n) = -\frac{i^n}{k_\mathrm{B}T}\frac{\delta^n H_\mathrm{w}}{\delta\mu_\mathrm{w}(\vec{q}_1), \ldots, \delta\mu_\mathrm{w}(\vec{q}_n)}\bigg|_{\mu_\mathrm{w}=0} \quad (18)$$

$$\mathbb{G}^{(n)}_{i1,\ldots,\mathrm{in}}(\vec{q}_1, \ldots, \vec{q}_n) = -\frac{i^n}{k_\mathrm{B}T}\frac{\delta^n H_\mathrm{p}}{\delta\mu_{i1}(\vec{q}_1), \ldots, \delta\mu_{in}(\vec{q}_n)}\bigg|_{\mu_\mathrm{A}=\mu_\mathrm{B}=0} \quad (19)$$

Here the Latin letters, $i1 = \{\mathrm{A}, \mathrm{B}\}$, ..., $in = \{\mathrm{A}, \mathrm{B}\}$. The first few order terms $\mathbb{G}^{(n)}_{\mathrm{w},\ldots,\mathrm{w}}$ for the solvent part are

$$\mathbb{G}^{(1)}_\mathrm{w}(\vec{q}_1) = n_\mathrm{w}\langle e^{i\vec{q}_1\cdot\vec{r}}\rangle_\mathrm{w} = 0 \quad (20)$$

$$\mathbb{G}^{(2)}_{\mathrm{ww}}(\vec{q}_1, \vec{q}_2) = n_\mathrm{w}\langle e^{i(\vec{q}_1+\vec{q}_2)\cdot\vec{r}}\rangle_\mathrm{w} = (2\pi)^3\delta(\vec{q}_1 + \vec{q}_2)\bar{\psi}_\mathrm{w} \quad (21)$$

$$\mathbb{G}^{(3)}_{\mathrm{www}}(\vec{q}_1, \vec{q}_2, \vec{q}_3) = n_\mathrm{w}\langle e^{i(\vec{q}_1+\vec{q}_2+\vec{q}_3)\cdot\vec{r}}\rangle_\mathrm{w} = (2\pi)^3\delta(\vec{q}_1 + \vec{q}_2 + \vec{q}_3)\bar{\psi}_\mathrm{w} \quad (22)$$

$$\mathbb{G}^{(4)}_{\mathrm{wwww}}(\vec{q}_1, \vec{q}_2, \vec{q}_3, \vec{q}_4) = n_\mathrm{w}\langle e^{i(\vec{q}_1+\vec{q}_2+\vec{q}_3++\vec{q}_4)\cdot\vec{r}}\rangle_\mathrm{w} = (2\pi)^3\delta(\vec{q}_1 + \vec{q}_2 + \vec{q}_3 + \vec{q}_4)\bar{\psi}_\mathrm{w} \quad (23)$$

where

$$\langle\hat{O}\rangle_\mathrm{w} \equiv \frac{\int d\vec{r}\hat{O}}{\int d\vec{r}} \quad (24)$$

The first few order terms $\mathbb{G}^{(n)}_{i1,\ldots,in}$ for the polymer part are

$$\mathbb{G}^{(1)}_i(\vec{q}_1) = n_\mathrm{p}\int ds_1\sigma_i(s_1)\langle e^{i\vec{q}_1\cdot\vec{R}(s)}\rangle_\mathrm{p} = 0 \quad (25)$$

$$\mathbb{G}^{(2)}_{ij}(\vec{q}_1, \vec{q}_2) = (2\pi)^3\delta(\vec{q}_1 + \vec{q}_2)N\bar{\psi}_\mathrm{M} \times \int\frac{ds_1}{N}\frac{ds_2}{N}\sigma_i(s_1)\sigma_j(s_2)\langle e^{i(\vec{q}_1\cdot\vec{R}(s_1)+\vec{q}_2\cdot\vec{R}(s_2))}\rangle_\mathrm{p} \quad (26)$$

$$\mathbb{G}^{(3)}_{ijk}(\vec{q}_1, \vec{q}_2, \vec{q}_3) = (2\pi)^3\delta(\vec{q}_1 + \vec{q}_2 + \vec{q}_3)N^2\bar{\psi}_\mathrm{M} \times \int\frac{ds_1}{N}\frac{ds_2}{N}\frac{ds_3}{N}\sigma_i(s_1)\sigma_j(s_2)\sigma_k(s_3) \times \langle e^{i(\vec{q}_1\cdot\vec{R}(s_1)+\vec{q}_2\cdot\vec{R}(s_2)+\vec{q}_3\cdot\vec{R}(s_3))}\rangle_\mathrm{p} \quad (27)$$

$$\mathbb{G}^{(4)}_{ijkl}(\vec{q}_1, \vec{q}_2, \vec{q}_3, \vec{q}_4) = (2\pi)^3\delta(\vec{q}_1 + \vec{q}_2 + \vec{q}_3 + \vec{q}_4)N^3\bar{\psi}_\mathrm{M} \times \int\frac{ds_1}{N}\frac{ds_2}{N}\frac{ds_3}{N}\frac{ds_4}{N}\sigma_i(s_1)\sigma_j(s_2)\sigma_k(s_3)\sigma_l(s_4) \times \langle e^{i(\vec{q}_1\cdot\vec{R}(s_1)+\vec{q}_2\cdot\vec{R}(s_2)+\vec{q}_3\cdot\vec{R}(s_3)+\vec{q}_4\cdot\vec{R}(s_4))}\rangle_\mathrm{p} \quad (28)$$

where $\bar{\psi}_\mathrm{M} = \bar{\psi}_\mathrm{A} + \bar{\psi}_\mathrm{B}$ and

$$\langle\hat{O}\rangle_\mathrm{p} \equiv \frac{\int\mathcal{D}\{\vec{R}(s)\}\hat{O}\exp\left[-\frac{3}{2l^2}\int ds\left(\frac{\partial\vec{R}(s)}{\partial s}\right)^2\right]}{\int\mathcal{D}\{\vec{R}(s)\}\exp\left[-\frac{3}{2l^2}\int ds\left(\frac{\partial\vec{R}(s)}{\partial s}\right)^2\right]} \quad (29)$$

Equation 25 is zero because the fluctuations in the microscopic variables $\hat{\psi}(\vec{q})$ should disappear over the whole space. The nonzero terms given in eqs 26−28 satisfy momentum conservation, namely, $\vec{q}_1 + \vec{q}_2 = 0$, $\vec{q}_1 + \vec{q}_2 + \vec{q}_3 = 0$, and $\vec{q}_1 + \vec{q}_2 + \vec{q}_3 + \vec{q}_4 = 0$ in eqs 26−28, respectively. The exact evaluations of $\mathbb{G}^{(n)}$ are listed in the Supporting Information.

2.4. Coarse-Grained-Effective Partition Function. Even though $H/k_\mathrm{B}T$ is a series, the integral over $\mathcal{D}\{\mu\}$ cannot be evaluated. Therefore, we use the saddle point approximation

$$\int_{\vec{q}\neq 0}\mathcal{D}\{\mu_\mathrm{w}(\vec{q})\}\exp\left[i\int_{\vec{q}\neq 0}\frac{d\vec{q}}{(2\pi)^3}\mu_\mathrm{w}(\vec{q})\psi_\mathrm{w}(-\vec{q}) - \frac{H_\mathrm{w}}{k_\mathrm{B}T}\right] \approx \exp\left[-\frac{F_\mathrm{w}}{k_\mathrm{B}T}\right] \quad (30)$$

$$\int_{\vec{q}\neq 0}\mathcal{D}\{\mu_\mathrm{A}(\vec{q})\}\mathcal{D}\{\mu_\mathrm{B}(\vec{q})\} \times \exp\left[i\int_{\vec{q}\neq 0}\frac{d\vec{q}}{(2\pi)^3}(\mu_\mathrm{A}(\vec{q})\psi_\mathrm{A}(-\vec{q}) + \mu_\mathrm{B}(\vec{q})\psi_\mathrm{B}(-\vec{q})) - \frac{H_\mathrm{p}}{k_\mathrm{B}T}\right] \approx \exp\left[-\frac{F_\mathrm{p}}{k_\mathrm{B}T}\right] \quad (31)$$

where $F_\mathrm{w}/k_\mathrm{B}T(\{\psi_\mathrm{w}\})$ and $F_\mathrm{p}/k_\mathrm{B}T(\{\psi_\mathrm{A}\}, \{\psi_\mathrm{B}\})$ are

$$\frac{F_\mathrm{w}}{k_\mathrm{B}T} \equiv \min_{\mu_\mathrm{w}}\left(\frac{H_\mathrm{w}}{k_\mathrm{B}T} - i\int_{\vec{q}\neq 0}\frac{d\vec{q}}{(2\pi)^3}\mu_\mathrm{w}(\vec{q})\psi_\mathrm{w}(-\vec{q})\right) \rightarrow \frac{-i}{k_\mathrm{B}T}\frac{\delta H_\mathrm{w}}{\delta\mu_\mathrm{w}} = \psi_\mathrm{w} \quad (32)$$

$$\frac{F_\mathrm{p}}{k_\mathrm{B}T} \equiv \min_{\mu_\mathrm{A},\mu_\mathrm{B}}\left(\frac{H_\mathrm{p}}{k_\mathrm{B}T} - i\int_{\vec{q}\neq 0}\frac{d\vec{q}}{(2\pi)^3}(\mu_\mathrm{A}(\vec{q})\psi_\mathrm{A}(-\vec{q}) + \mu_\mathrm{B}(\vec{q})\psi_\mathrm{B}(-\vec{q}))\right) \rightarrow \frac{-i}{k_\mathrm{B}T}\frac{\delta H_\mathrm{p}}{\delta\mu_{\mathrm{A(B)}}} = \psi_{\mathrm{A(B)}} \quad (33)$$

Expressing $F/k_\mathrm{B}T$ as a series, we obtain

$$\frac{F_\mathrm{w}}{k_\mathrm{B}T} = (\ln n_\mathrm{w}! - n_\mathrm{w}\ln\Omega) + \sum_{n=2}\frac{(-1)^n}{n!}\int_{\vec{q}\neq 0}\frac{d\vec{q}_1}{(2\pi)^3}, \ldots, \frac{d\vec{q}_n}{(2\pi)^3}\Gamma^{(n)}_{\mathrm{w},\ldots,\mathrm{w}}(\vec{q}_1, \ldots, \vec{q}_n)\overbrace{\psi_\mathrm{w}(\vec{q}_1), \ldots, \psi_\mathrm{w}(\vec{q}_n)}^{n} \quad (34)$$

$$\frac{F_\mathrm{p}}{k_\mathrm{B}T} = (\ln n_\mathrm{p}! - n_\mathrm{p}\ln\Omega) + \sum_{n=2}\frac{(-1)^n}{n!}\sum_{i1=\{\mathrm{A},\mathrm{B}\}}, \ldots, \sum_{in=\{\mathrm{A},\mathrm{B}\}}\int_{\vec{q}\neq 0}\frac{d\vec{q}_1}{(2\pi)^3}, \ldots, \frac{d\vec{q}_n}{(2\pi)^3}\Gamma^{(n)}_{i1,\ldots,in}(\vec{q}_1, \ldots, \vec{q}_n)\psi_{i1}(\vec{q}_1), \ldots, \psi_{in}(\vec{q}_n) \quad (35)$$

By the standard method,[54] the first few order terms $\Gamma^{(n)}$ are

$$\Gamma^{(2)}_{\mathrm{ww}}(\vec{q}_1, \vec{q}_2) = (\mathbb{G}^{(2)})^{-1}_{\mathrm{ww}} = (2\pi)^3\delta(\vec{q}_1 + \vec{q}_2)\frac{1}{\bar{\psi}_\mathrm{w}} \quad (36)$$

https://doi.org/10.1021/acs.macromol.2c00008
Macromolecules 2022, 55, 5535−5549

$$\Gamma^{(3)}_{www}(\vec{q}_1, \vec{q}_2, \vec{q}_3) = \int \frac{d\vec{q}_1'}{(2\pi)^3}\frac{d\vec{q}_2'}{(2\pi)^3}\frac{d\vec{q}_3'}{(2\pi)^3}(\mathbb{G}^{(2)})^{-1}_{ww}(\vec{q}_1, \vec{q}_1') \times (\mathbb{G}^{(2)})^{-1}_{ww}(\vec{q}_2, \vec{q}_2')(\mathbb{G}^{(2)})^{-1}_{ww}(\vec{q}_3, \vec{q}_3') \times \mathbb{G}^{(3)}_{www}(\vec{q}_1', \vec{q}_2', \vec{q}_3') = (2\pi)^3\delta(\vec{q}_1 + \vec{q}_2 + \vec{q}_3)\frac{1}{\bar{\psi}_w^2} \tag{37}$$

$$\begin{aligned}\Gamma^{(4)}_{wwww}(\vec{q}_1, \vec{q}_2, \vec{q}_3, \vec{q}_4) &= \int \frac{d\vec{q}_1'}{(2\pi)^3}\frac{d\vec{q}_2'}{(2\pi)^3}\frac{d\vec{q}_3'}{(2\pi)^3}\frac{d\vec{q}_4'}{(2\pi)^3}(\mathbb{G}^{(2)})^{-1}_{ww}(\vec{q}_1, \vec{q}_1')(\mathbb{G}^{(2)})^{-1}_{ww}(\vec{q}_1, \vec{q}_1')(\mathbb{G}^{(2)})^{-1}_{ww}(\vec{q}_2, \vec{q}_2')(\mathbb{G}^{(2)})^{-1}_{ww}(\vec{q}_3, \vec{q}_3')(\mathbb{G}^{(2)})^{-1}_{ww}(\vec{q}_4, \vec{q}_4') \times \Big\{-\mathbb{G}^{(4)}_{wwww}(\vec{q}_1', \vec{q}_2', \vec{q}_3', \vec{q}_4') \\ &+ \int \frac{d\vec{q}_5'}{(2\pi)^3}\frac{d\vec{q}_6'}{(2\pi)^3}[\mathbb{G}^{(3)}_{www}(\vec{q}_1', \vec{q}_2', \vec{q}_5')(\mathbb{G}^{(2)})^{-1}_{ww}(\vec{q}_5', \vec{q}_6')\mathbb{G}^{(3)}_{www}(\vec{q}_6', \vec{q}_3', \vec{q}_4') + \mathbb{G}^{(3)}_{www}(\vec{q}_1', \vec{q}_3', \vec{q}_5')(\mathbb{G}^{(2)})^{-1}_{ww}(\vec{q}_5', \vec{q}_6')\mathbb{G}^{(3)}_{www}(\vec{q}_6', \vec{q}_2', \vec{q}_4') + \mathbb{G}^{(3)}_{www}(\vec{q}_1', \vec{q}_4', \vec{q}_5')(\mathbb{G}^{(2)})^{-1}_{ww}(\vec{q}_5', \vec{q}_6')\mathbb{G}^{(3)}_{www}(\vec{q}_6', \vec{q}_2', \vec{q}_3')]\Big\} \\ &= (2\pi)^3\delta(\vec{q}_1 + \vec{q}_2 + \vec{q}_3 + \vec{q}_4)\frac{2}{\bar{\psi}_w^3}\end{aligned} \tag{38}$$

and

$$\Gamma^{(2)}_{ij}(\vec{q}_1, \vec{q}_2) = (\mathbb{G}^{(2)})^{-1}_{ij} \tag{39}$$

$$\Gamma^{(3}_{ijk}(\vec{q}_1, \vec{q}_2, \vec{q}_3) = (\mathbb{G}^{(2)})^{-1}_{ii'}(\mathbb{G}^{(2)})^{-1}_{jj'}(\mathbb{G}^{(2)})^{-1}_{kk'}\mathbb{G}^{(3)}_{i'j'k'} \tag{40}$$

$$\begin{aligned}\Gamma^{(4)}_{ijkl}(\vec{q}_1, \vec{q}_2, \vec{q}_3, \vec{q}_4) &= (\mathbb{G}^{(2)})^{-1}_{ii'}(\mathbb{G}^{(2)})^{-1}_{jj'}(\mathbb{G}^{(2)})^{-1}_{kk'}(\mathbb{G}^{(2)})^{-1}_{ll'} \times [-\mathbb{G}^{(4)}_{i'j'k'l'} \\ &+ \mathbb{G}^{(3)}_{i'j'm}(\mathbb{G}^{(2)})^{-1}_{mn}\mathbb{G}^{(3)}_{nk'l'} + \mathbb{G}^{(3)}_{i'k'm}(\mathbb{G}^{(2)})^{-1}_{mn}\mathbb{G}^{(3)}_{mj'l'} + \mathbb{G}^{(3)}_{i'l'm} (\mathbb{G}^{(2)})^{-1}_{mn}\mathbb{G}^{(3)}_{nj'k'}]\end{aligned} \tag{41}$$

where the Dirac delta functions in $\Gamma^{(n)}$ or $\mathbb{G}^{(n)}$ in eqs 39−41 are suppressed because it will be integrated out as shown in eqs 36−38. Consequently, the Dirac delta functions of momenta are replaced by the conservation law $\vec{q}_1 + \vec{q}_2 = 0$, $\vec{q}_1 + \vec{q}_2 + \vec{q}_3 = 0$, and $\vec{q}_1 + \vec{q}_2 + \vec{q}_3 + \vec{q}_4 = 0$ in eq 39, eq 40, and eq 41, respectively. The Einstein's convention is implemented in eqs 39−41 and the following paragraphs. In the above equations, the momentum dependence of $\mathbb{G}$ is dropped for the sake of simplification of presentation. However, the $\mathbb{G}^{(3)}_{ijk}(\vec{q}_1, \vec{q}_2, \vec{q}_3) \neq \mathbb{G}^{(3)}_{ijk}(\vec{q}_2, \vec{q}_1, \vec{q}_3)$ in general. To avoid such confusions, the following convention is adopted: The momentum of species i is $\vec{q}_1$, the momentum of species j is $\vec{q}_2$, and so on. The momentum dependence of other quantities, if they are dependent on momentum, are passed by contracted indices. For example, in $\mathbb{G}^{(3)}_{ijk}(\vec{q}_1, \vec{q}_2, \vec{q}_3)f_i$, the momentum dependence of f_i is $\vec{q}_1$, namely, $f_i(\vec{q}_1)$. To provide an example of this convention, eq 40 should be read as

$$\begin{aligned}\Gamma^{(3)}_{ijk}(\vec{q}_1, \vec{q}_2, \vec{q}_3) &= (\mathbb{G}^{(2)})^{-1}_{ii'}(\vec{q}_1, -\vec{q}_1)(\mathbb{G}^{(2)})^{-1}_{jj'}(\vec{q}_2, -\vec{q}_2)(\mathbb{G}^{(2)})^{-1}_{kk'} \\ &\times (\vec{q}_3, -\vec{q}_3)\mathbb{G}^{(3)}_{i'j'k'}(-\vec{q}_1, -\vec{q}_2, -\vec{q}_3)\end{aligned} \tag{42}$$

The result in eq 35 is an effective interaction based on the Gaussian chain assumption.[39] The physical picture behind the equation is that the chain connectivity among monomers is transformed into the effective interactions among density fields. The effective partition function $\mathcal{Z}_{eff}$ is

$$\begin{aligned}\mathcal{Z} &\approx \mathcal{Z}_{eff} \\ &= \int \mathcal{D}\{\psi_w(0)\}\mathcal{D}\{\psi_A(0)\}\mathcal{D}\{\psi_B(0)\} \\ &\times \delta[\psi_w(0) + \psi_A(0) + \psi_B(0) - \Omega] \\ &\times \delta[\psi_w(0) - \Omega\bar{\psi}_w]\delta[\psi_A(0) - \Omega\bar{\psi}_A]\delta[\psi_B(0) - \Omega\bar{\psi}_B] \\ &\times \int_{\vec{q}\neq 0}\mathcal{D}\{\psi_w(\vec{q})\}\mathcal{D}\{\psi_A(\vec{q})\}\mathcal{D}\{\psi_B(\vec{q})\} \times \\ &\prod_{\vec{q}\neq 0}\delta[\psi_w(\vec{q}) + \psi_A(\vec{q}) + \psi_B(\vec{q})] \\ &\times \exp\left[-\frac{F_w}{k_BT} - \frac{F_p}{k_BT} - \frac{U}{k_BT}\right]\end{aligned} \tag{43}$$

Rewriting $U(\{\psi_w\}, \{\psi_A\}, \{\psi_B\})/k_BT$ in the momentum space, we get

$$\begin{aligned}\frac{U}{k_BT} &= \frac{U_0}{k_BT} + \Omega\left(\chi_{Aw}\bar{\psi}_A\bar{\psi}_w + \chi_{Bw}\bar{\psi}_B\bar{\psi}_w + \chi_{AB}\bar{\psi}_A\bar{\psi}_B + \frac{2\pi z_p^2 l_B}{\kappa^2}\bar{\psi}_B^2\right) \\ &+ \frac{1}{2!}\sum_{\alpha=\{w,A,B\}}\sum_{\beta=\{w,A,B\}}\int_{\vec{q}\neq 0}\frac{d\vec{q}_1}{(2\pi)^3}\frac{d\vec{q}_2}{(2\pi)^3}V_{\alpha\beta}(\vec{q}_1, \vec{q}_2) \times \psi_\alpha(\vec{q}_1)\psi_\beta(\vec{q}_2)\end{aligned} \tag{44}$$

where $V_{\alpha\beta}$ are interactions in momentum space

$$V_{\alpha\beta}(\vec{q}_1, \vec{q}_2) = (2\pi)^3\delta(\vec{q}_1 + \vec{q}_2)\begin{pmatrix} 0 & \chi_{Aw} & \chi_{Bw} \\ \chi_{Aw} & 0 & \chi_{AB} \\ \chi_{Bw} & \chi_{AB} & \frac{4\pi z_p^2 l_B}{q_1^2 + \kappa^2}\end{pmatrix} \tag{45}$$

Using the eqs 34, 35, and 44, $\mathcal{Z}(\vec{q} = 0) \equiv \mathcal{Z}_{mean}$ is

$$\mathcal{Z}_{mean} = \text{cst} \times \exp\left[-\Omega\left(\frac{\bar{\psi}_M}{N}\ln(\bar{\psi}_M) + \bar{\psi}_w \ln\bar{\psi}_w + \chi_{Aw}\bar{\psi}_A\bar{\psi}_w + \chi_{Bw}\bar{\psi}_B\bar{\psi}_w + \chi_{AB}\bar{\psi}_A\bar{\psi}_B + \frac{2\pi z_p^2 l_B}{\kappa^2}\bar{\psi}_B^2\right)\right] \tag{46}$$

where cst stands for a numerical prefactor that is of no physical consequence. Therefore, $\mathcal{Z}_{eff}$ of eq 43 is given by

https://doi.org/10.1021/acs.macromol.2c00008
Macromolecules 2022, 55, 5535−5549

$$\frac{\mathcal{Z}_{\text{eff}}}{\mathcal{Z}_{\text{mean}}} = \int_{\vec{q}\neq 0} \mathcal{D}\{\psi_{\text{w}}(\vec{q})\}\mathcal{D}\{\psi_{\text{A}}(\vec{q})\}\mathcal{D}\{\psi_{\text{B}}(\vec{q})\} \times \prod_{\vec{q}\neq 0} \delta[\psi_{\text{w}}(\vec{q}) + \psi_{\text{A}}(\vec{q}) + \psi_{\text{B}}(\vec{q})] \times \exp\left[-\frac{1}{2!}\int(\Gamma^{(2)}_{\alpha\beta} + V_{\alpha\beta})\psi_\alpha\psi_\beta + \frac{1}{3!}\int\Gamma^{(3)}_{\alpha\beta\gamma}\psi_\alpha\psi_\beta\psi_\gamma - \frac{1}{4!}\int\Gamma^{(4)}_{\alpha\beta\gamma\delta}\psi_\alpha\psi_\beta\psi_\gamma\psi_\delta + \ldots\right] \tag{47}$$

$$\approx \int_{\vec{q}\neq 0} \mathcal{D}\{\psi_{\text{A}}(\vec{q})\}\mathcal{D}\{\psi_{\text{B}}(\vec{q})\} \times \exp\left[-\frac{1}{2!}\int(\Gamma^{(2)}_{\alpha\beta} + V_{\alpha\beta}) \times h_{\alpha i}h_{\beta j}\psi_i\psi_j + \frac{1}{3!}\int\Gamma^{(3)}_{\alpha\beta\gamma}h_{\alpha i}h_{\beta j} \times h_{\gamma k}\psi_i\psi_j\psi_k - \frac{1}{4!}\int\Gamma^{(4)}_{\alpha\beta\gamma\delta}h_{\alpha i}h_{\beta j}h_{\gamma k}h_{\delta l}\psi_i\psi_j\psi_k\psi_l\right] \tag{48}$$

where the first few order terms $\Gamma^{(n)}$ are

$$\Gamma^{(2)}_{\alpha\beta} = \begin{cases} 1/\bar{\psi}_{\text{w}} & \alpha = \beta = \text{w} \\ \Gamma^{(2)}_{ij} & \alpha = i \text{ and } \beta = j \\ 0 & \text{otherwise} \end{cases} \tag{49}$$

$$\Gamma^{(3)}_{\alpha\beta\gamma} = \begin{cases} 1/\bar{\psi}^2_{\text{w}} & \alpha = \beta = \gamma = \text{w} \\ \Gamma^{(3)}_{ijk} & \alpha = i, \beta = j, \text{ and } \gamma = k \\ 0 & \text{otherwise} \end{cases} \tag{50}$$

$$\Gamma^{(4)}_{\alpha\beta\gamma\delta} = \begin{cases} 2/\bar{\psi}^3_{\text{w}} & \alpha = \beta = \gamma = \delta = \text{w} \\ \Gamma^{(4)}_{ijkl} & \alpha = i, \beta = j, \gamma = k, \text{ and } \delta = l \\ 0 & \text{otherwise} \end{cases} \tag{51}$$

Here, Einstein's convention is implemented, the Greek letters α, β, γ, and δ are indices of {w, A, B}, the Latin letters i, j, k, and l are indices of {A, B}, the $d\vec{q}$ are not written down explicitly for simplification, the Dirac delta functions are suppressed, and the momentum of species α is $\vec{q}_1$, the momentum of species β is $\vec{q}_2$, and so on. In addition, the incompressibility constraint reduces the number of independent parameters, so that $(\psi_{\text{w}}, \psi_{\text{A}}, \psi_{\text{B}})$ is reduced to $(-\psi_{\text{A}} - \psi_{\text{B}}, \psi_{\text{A}}, \psi_{\text{B}})$. The $h_{\alpha i}$ in eq 48 is

$$h_{\alpha i} = \begin{pmatrix} -1 & 1 & 0 \\ -1 & 0 & 1 \end{pmatrix} \tag{52}$$

The exponent of eq 48 gives us the Landau free energy in terms of ψ_ω and the information on the sequences (eq 5) is incorporated in $\Gamma^{(n)}$.

2.5. Coarse-Grained-Effective-Reduced Partition Function. We obtain the phase behavior of the system by truncating the partition function in eq 48 at the fourth order of the free energy F. If the minimum of F is smaller than 0 at $(\psi^*_{\text{A}}(\vec{q}^*), \psi^*_{\text{B}}(\vec{q}^*))$, the instability will occur around the size of $1/|\vec{q}^*|$ with formation of an ordered microphase with a specific morphology.

In order to determine the minimum of F, it is convenient to diagonalize $(\Gamma^{(2)}_{\alpha\beta} + V_{\alpha\beta})h_{\alpha i}h_{\beta j}$, which is a 2 × 2 matrix in the model. As a result, there are two eigenvalues λ_{g} and λ_{e} along two eigenvectors

$$\vec{u}^{(\text{g})}(\vec{q}) = (\psi^{(\text{g})}_{\text{A}}(\vec{q}), \psi^{(\text{g})}_{\text{B}}(\vec{q}))/\sqrt{|\psi^{(\text{g})}_{\text{A}}|^2 + |\psi^{(\text{g})}_{\text{B}}|^2}$$
$$\vec{u}^{(\text{e})}(\vec{q}) = (\psi^{(\text{e})}_{\text{A}}(\vec{q}), \psi^{(\text{e})}_{\text{B}}(\vec{q}))/\sqrt{|\psi^{(\text{e})}_{\text{A}}|^2 + |\psi^{(\text{e})}_{\text{B}}|^2} \tag{53}$$

respectively. The two eigenvalues are good indicators of microphase separation transition (MST) because the shape of F will be a Mexican hat if one of them is negative. Furthermore, if both of them are negative, it will correspond to the two-length-scale microphase separation. However, under the weak segregation limit (WSL), there is only one scale for the formation of microdomains. Assume, without the loss of generality, $\lambda_{\text{e}} > 0$ and $\lambda_{\text{g}} \sim 0$ in WSL and

$$(\psi_{\text{A}}(\vec{q}), \psi_{\text{B}}(\vec{q})) = \Psi_{\text{g}}\vec{u}^{(\text{g})}(\vec{q}) + \Psi_{\text{e}}\vec{u}^{(\text{e})}(\vec{q}) \tag{54}$$

where the $\Psi_{\text{g(e)}}$ is the strength of fluctuations along $\vec{u}^{(\text{g(e)})}$. Because $\lambda_{\text{e}} > \lambda_{\text{g}}$, the weak fluctuations Ψ_{e} can be integrated out. Therefore, the reduced partition function (the derivation is in the Supporting Information) becomes

$$\frac{\mathcal{Z}_{\text{eff}}}{\mathcal{Z}_{\text{mean}}} \approx \frac{\mathcal{Z}_{\text{reduced}}}{\mathcal{Z}_{\text{mean}}} = \int \mathcal{D}\{\Psi_{\text{g}}(\vec{q})\}\exp\left[-\frac{F_{\text{g}}}{k_{\text{B}}T}\right] \tag{55}$$

where F_{g}[55] is

$$\frac{F_{\text{g}}}{k_{\text{B}}T} = \frac{1}{2!}\int\lambda_{\text{g}}\Psi_{\text{g}}(\vec{q}_1)\Psi_{\text{g}}(\vec{q}_2) - \frac{1}{3!}\int\Gamma^{(3)}_{\text{g}}\Psi_{\text{g}}(\vec{q}_1)\Psi_{\text{g}}(\vec{q}_2)\Psi_{\text{g}}(\vec{q}_3) + \frac{1}{4!}\int\Gamma^{(4)}_{\text{g}}\Psi_{\text{g}}(\vec{q}_1)\Psi_{\text{g}}(\vec{q}_2)\Psi_{\text{g}}(\vec{q}_3)\Psi_{\text{g}}(\vec{q}_4) \tag{56}$$

Here, the $\Gamma^{(3)}_{\text{g}}$ and $\Gamma^{(4)}_{\text{g}}$ are

$$\Gamma^{(3)}_{\text{g}} = \Gamma^{(3)}_{\alpha\beta\gamma}h_{\alpha i}h_{\beta j}h_{\gamma k}u^{(\text{g})}_i u^{(\text{g})}_j u^{(\text{g})}_k \tag{57}$$

$$\begin{aligned}\Gamma^{(4)}_{\text{g}} = {} & \Gamma^{(4)}_{\alpha\beta\gamma\delta}h_{\alpha i}h_{\beta j}h_{\gamma k}h_{\delta l}u^{(\text{g})}_i u^{(\text{g})}_j u^{(\text{g})}_k u^{(\text{g})}_l \\ & - [\Gamma^{(3)}_{\alpha\beta\epsilon}h_{\alpha i}h_{\beta j}h_{\epsilon e}u^{(\text{g})}_i u^{(\text{g})}_j u^{(\text{e})}_{\text{e}}(-\vec{q}_1 - \vec{q}_2)] \\ & \times [\Gamma^{(3)}_{\gamma\delta\zeta}h_{\gamma k}h_{\delta l}h_{\zeta f}u^{(\text{g})}_k u^{(\text{g})}_l u^{(\text{e})}_f(-\vec{q}_3 - \vec{q}_4)]/\lambda_{\text{e}} \\ & - [\Gamma^{(3)}_{\alpha\gamma\epsilon}h_{\alpha i}h_{\gamma k}h_{\epsilon e}u^{(\text{g})}_i u^{(\text{g})}_k u^{(\text{e})}_{\text{e}}(-\vec{q}_1 - \vec{q}_3)] \\ & \times [\Gamma^{(3)}_{\beta\delta\zeta}h_{\beta j}h_{\delta l}h_{\zeta f}u^{(\text{g})}_j u^{(\text{g})}_l u^{(\text{e})}_f(-\vec{q}_2 - \vec{q}_4)]/\lambda_{\text{e}} \\ & - [\Gamma^{(3)}_{\alpha\delta\epsilon}h_{\alpha i}h_{\delta l}h_{\epsilon e}u^{(\text{g})}_i u^{(\text{g})}_l u^{(\text{e})}_{\text{e}}(-\vec{q}_1 - \vec{q}_4)] \\ & \times [\Gamma^{(3)}_{\beta\gamma\zeta}h_{\beta j}h_{\gamma k}h_{\zeta f}u^{(\text{g})}_j u^{(\text{g})}_k u^{(\text{e})}_f(-\vec{q}_2 - \vec{q}_3)]/\lambda_{\text{e}}\end{aligned} \tag{58}$$

where the conventions are the same as those below eq 51. By writing down the momenta of $u^{(\text{e})}$ explicitly, an example is

$$\begin{aligned}&\Gamma^{(3)}_{\alpha\beta\epsilon}h_{\alpha i}h_{\beta j}h_{\epsilon e}u^{(\text{g})}_i u^{(\text{g})}_j u^{(\text{e})}_{\text{e}}(-\vec{q}_1 - \vec{q}_2) \\ &= \Gamma^{(3)}_{\alpha\beta\epsilon}(\vec{q}_1, \vec{q}_2, -\vec{q}_1 - \vec{q}_2)h_{\alpha i}h_{\beta j}h_{\epsilon e}u^{(\text{g})}_i(\vec{q}_1)u^{(\text{g})}_j(\vec{q}_2) \\ &\quad \times u^{(\text{e})}_{\text{e}}(-\vec{q}_1 - \vec{q}_2)\end{aligned} \tag{59}$$

and so on. The morphology phase diagrams are calculated from F_{g} given in eq 55.

https://doi.org/10.1021/acs.macromol.2c00008
Macromolecules 2022, 55, 5535−5549

3. RESULTS AND DISCUSSION

3.1. Stability Limit of the Disordered Phase. The limit of stability of the disordered phase against the formation of an ordered phase is given by the spinodal point at which $\lambda_g = 0$. In general, λ_g is the inverse of the structure factor (proportional to the scattering intensity in scattering experiments). As is well-known in block copolymer systems, the structure factor exhibits a scattering peak at a nonzero wavevector $|\vec{q}| = q^*$. Therefore, we define the spinodal point at the location in the parameter space at which $\lambda_g(q^*) = 0$. The criterion for spinodal points for the disorder−order transition (DOT) is thus given as

$$\min_{\vec{q},\chi_{AB}} \lambda_g = 0 \tag{60}$$

which occurs if and only if

$$\min_{\vec{q},\chi_{AB}} \det(\Gamma^{(2)}_{\alpha\beta} + V_{\alpha\beta})h_{i\alpha}h_{j\beta} = 0 \tag{61}$$

where the minimization of λ_g is performed with respect to $\vec{q}$ and χ_{AB}. Combining eqs 45, 49, and 52, the matrix of the determinant is given by

$$\begin{aligned}(\Gamma^{(2)}_{\alpha\beta} + V_{\alpha\beta})h_{i\alpha}h_{j\beta} &= \begin{pmatrix}-1 & 1 & 0\\ -1 & 0 & 1\end{pmatrix}\left[\begin{pmatrix}1/\bar{\psi}_w & 0 & 0\\ 0 & \frac{\mathbb{G}^{(2)}_{BB}}{\det(\mathbb{G}^{(2)})} & \frac{-\mathbb{G}^{(2)}_{AB}}{\det(\mathbb{G}^{(2)})}\\ 0 & \frac{-\mathbb{G}^{(2)}_{BA}}{\det(\mathbb{G}^{(2)})} & \frac{\mathbb{G}^{2}_{AA}}{\det(\mathbb{G}^{(2)})}\end{pmatrix} + \begin{pmatrix}0 & \chi_{Aw} & \chi_{Bw}\\ \chi_{Aw} & 0 & \chi_{AB}\\ \chi_{Bw} & \chi_{AB} & \frac{4\pi\alpha^2 l_B}{q_1^2+\kappa^2}\end{pmatrix}\right]\begin{pmatrix}-1 & -1\\ 1 & 0\\ 0 & 1\end{pmatrix}\\ &= \begin{pmatrix}\frac{\mathbb{G}^{(2)}_{BB}}{\det\mathbb{G}^{(2)}} & \frac{-\mathbb{G}^{(2)}_{AB}}{\det\mathbb{G}^{(2)}}\\ \frac{-\mathbb{G}^{(2)}_{BA}}{\det\mathbb{G}^{(2)}} & \frac{\mathbb{G}^{2}_{AA}}{\det\mathbb{G}^{(2)}}\end{pmatrix} + \begin{pmatrix}1/\bar{\psi}_w - 2\bar{\chi}_w & 1/\bar{\psi}_w - 2\bar{\chi}_w\\ 1/\bar{\psi}_w - 2\bar{\chi}_w & 1/\bar{\psi}_w - 2\bar{\chi}_w\end{pmatrix} + \begin{pmatrix}-2\Delta\chi & \chi_{AB}\\ \chi_{AB} & 2\Delta\chi + \frac{4\pi\alpha^2 l_B}{q^2+\kappa^2}\end{pmatrix}\end{aligned} \tag{62}$$

The corresponding determinant is

$$\begin{aligned}&\frac{1}{N^2}\left(\frac{N\sum\mathbb{G}^{(2)}}{\det\mathbb{G}^{(2)}} - 2N\chi_{AB} + N\nu_{el}\right)\left\{N\left(\frac{1}{\bar{\psi}_w} - 2\bar{\chi}_w\right)\right.\\ &+\left(1 - \frac{-2N\chi_{AB} + N\nu_{el}}{\frac{N\sum\mathbb{G}^{(2)}}{\det\mathbb{G}^{(2)}} - 2N\chi_{AB} + N\nu_{el}}\right)\\ &\times\left[\frac{N + 2N\Delta\chi(\mathbb{G}^{(2)}_{BB} - \mathbb{G}^{(2)}_{AA}) + 2N\chi_{AB}\mathbb{G}^{(2)}_{AB} + N\nu_{el}\mathbb{G}^{(2)}_{BB}}{\sum\mathbb{G}^{(2)}}\right.\\ &\left.\left.- \frac{(N\chi_{AB})^2 + 2N\Delta\chi(2N\Delta\chi + N\nu_{el})}{N\sum\mathbb{G}^{(2)}/\det\mathbb{G}^{(2)}}\right]\right\}\end{aligned} \tag{63}$$

where the $\mathbb{G}^{(2)}_{ij}$ are elements of $\mathbb{G}^{(2)}$, $\bar{\chi}_w \equiv (\chi_{Aw} + \chi_{Bw})/2$, $\Delta\chi \equiv (\chi_{Aw} - \chi_{Bw})/2$, $\nu_{el} \equiv 4\pi\alpha^2 l_B/(q^2+\kappa^2)$, and $\sum\mathbb{G}^{(2)} = \mathbb{G}^{(2)}_{AA} + \mathbb{G}^{(2)}_{AB} + \mathbb{G}^{(2)}_{BA} + \mathbb{G}^{(2)}_{BB}$. The q and χ_{AB} at spinodal points are denoted by q^* and χ^*_{AB}.

Two limits from eq 63 correspond to two well-known results. One is that the equation approaches the well-known melt results from RPA[36,39,40] as $\bar{\psi}_w$ approaches zero, and the other one is the result of liquid−liquid phase separation[56] if the polymers are uncharged and homopolymers, namely, $\chi_{AB} = \Delta\chi = \nu_{el} = 0$. The spinodal points of two different systems S and S′ are the same if $1/\bar{\psi}_w - 2\bar{\chi}_w = 1/\bar{\psi}'_w - 2\bar{\chi}'_w$. In addition, because the $\mathbb{G}^{(2)}_{ij}$ is proportional to N as shown in eq 26, there is a mapping relationship

$$\begin{aligned}&\left(N\chi_{AB}, N\Delta\chi, N\left(\frac{1}{\bar{\psi}_w} - 2\bar{\chi}_w\right), Nz_p^2 l_B, \kappa\right)\\ &\leftrightarrow \left(N'\chi'_{AB}, N'\Delta\chi', N'\left(\frac{1}{\bar{\psi}'_w} - 2\bar{\chi}'_w\right), N'z_p'^2 l'_B, \kappa'\right)\end{aligned} \tag{64}$$

This mapping helps to reduce the parameter space in constructing spinodal curves and morphology diagrams.

3.2. Sequence Dependence of Spinodal Points. For the simple system illustrated in the present paper, the key variables are N, z_p, l_B, κ, $\bar{\chi}_w$, $\Delta\chi$, χ_{AB}, $\bar{\psi}_w$, and the sequence. We fix the values of N, z_p, l_B, and $\bar{\chi}_w$ as given in Table 1. We vary κ, $\bar{\psi}_w$, and the sequence and determine their corresponding spinodal condition χ^*_{AB}. In terms of $\Delta\chi$ ($= (\chi_{Aw} - \chi_{Bw})/2$), we consider two cases: Case I, $\Delta\chi = 0$, corresponding to a common theta solvent for both A and B polymer segments; Case II, $\Delta\chi = 0.2$, corresponding to a selective solvent with $\chi_{Bw} = 0.3$ (good solvent for B segments) and $\chi_{Aw} = 0.7$ (poor solvent for A segments). Among the

Table 1. List of Parameters

N	200	Seq 1	$A_{50}A_{50}B_{50}B_{50}$ ($\eta = 1$)
z_p	0.3	Seq 2	$A_{50}B_{50}A_{50}B_{50}$ ($\eta = 1/3$)
lB	0.7l	Seq 3	$A_{50}B_{50}B_{50}A_{50}$ ($\eta = 1/2$)
$\bar{\chi}_w$	0.5	Seq 4	$B_{50}A_{50}A_{50}B_{50}$ ($\eta = 1/2$)
Case I			Case II
$\Delta\chi = 0$			$\Delta\chi = 0.2$

https://doi.org/10.1021/acs.macromol.2c00008
Macromolecules 2022, 55, 5535−5549

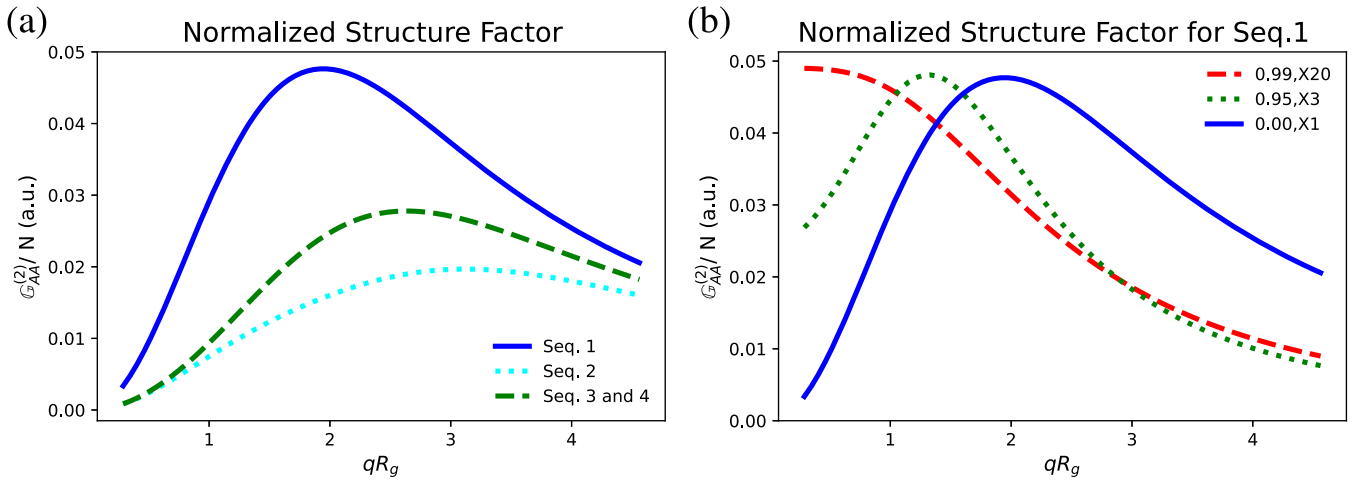

Figure 1. (a) Normalized structure factor of A monomers for Seqs 1−4 without solvent and interactions. (b) Normalized structure factor of A monomers for Seq 1 with $\bar{\psi}_w$ = 0.0, 0.95, and 0.99 for Case II without any potential interactions. In order to demonstrate q^*, the normalized structure factor is multiplied by 3 and 20 for $\bar{\psi}_w$ = 0.95 and 0.99, respectively.

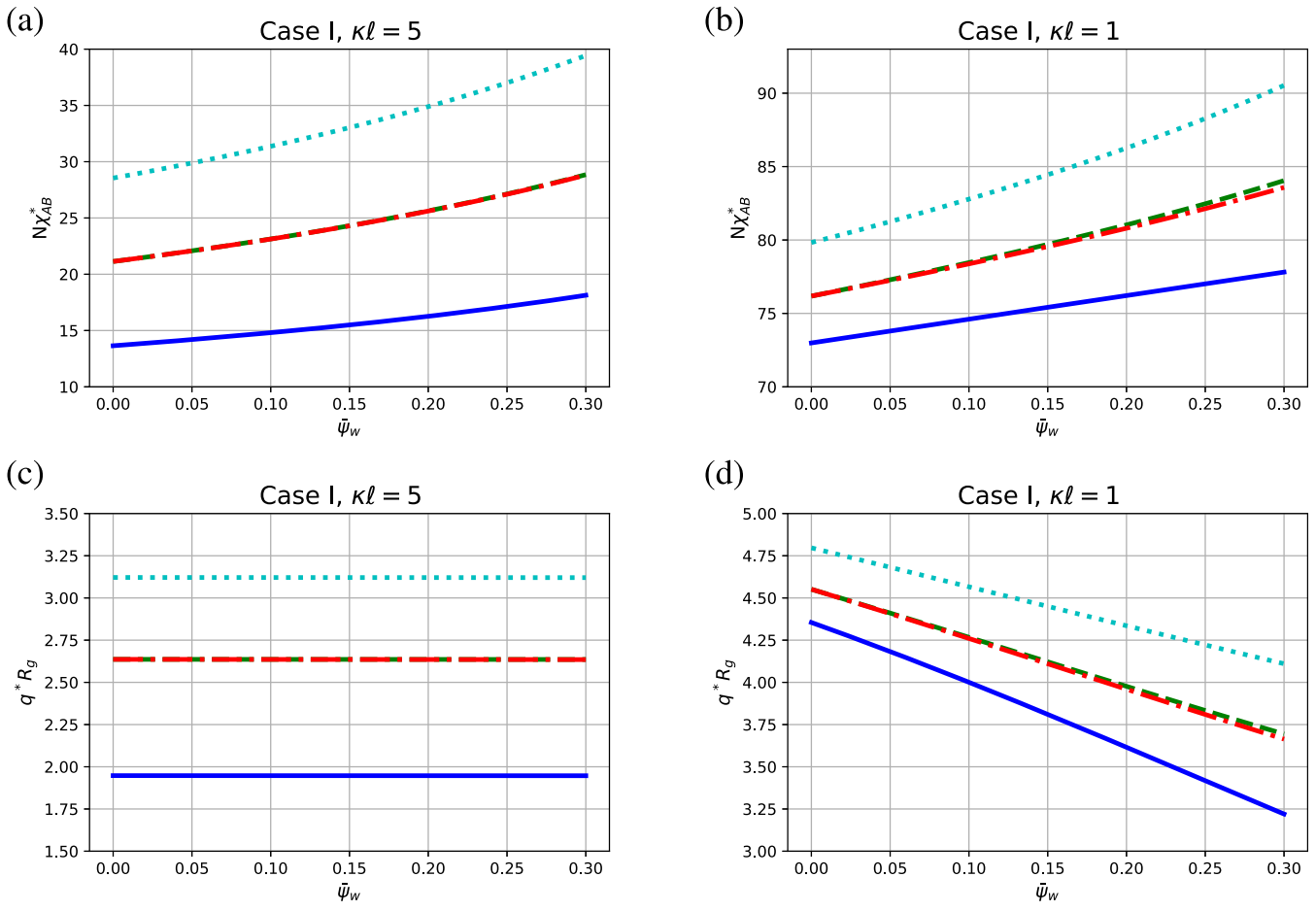

Figure 2. Spinodal values $N\chi^*_{AB}$ and the periodicity q^*R_g for Case I: Seq 1 (blue solid, —), Seq 2 (cyan dotted, ···), Seq 3 (green dashed, ---), and Seq 4 (red dash-dot, -·-·). (a) Plot of $N\chi^*_{AB}$ versus $\bar{\psi}_w$ at $\kappa l = 5$. The difference between Seq 3 and Seq 4 is not obvious in the scale. (b) Plot of $N\chi^*_{AB}$ versus = ψ_w for at $\kappa l = 1$. (c) and (d) are the plots of q^*R_g corresponding to (a) and (b), respectively.

enormous number of possible sequences, we consider only four sequences $A_{50}A_{50}B_{50}B_{50}$, $A_{50}B_{50}A_{50}B_{50}$, $A_{50}B_{50}B_{50}A_{50}$, and $B_{50}A_{50}A_{50}B_{50}$, labeled as Seq 1, Seq 2, Seq 3, and Seq 4, respectively (Table 1). We define the sequence order parameter η as the reciprocal of the number of domain walls separating two adjacent A and B blocks. The values of η for Seqs 1−4 are 1, 1/3, 1/2, and 1/2, respectively (Table 1). Even with such a simple variation in the sequences, their influences on the stability limit and formation of morphologies are significant as demonstrated below. We have chosen the range of the inverse Debye length κ between $\kappa l = 1$ and $\kappa l = 5$. For the segment length $l = 1$ nm, $\kappa l = 1$ and 5

https://doi.org/10.1021/acs.macromol.2c00008
Macromolecules 2022, 55, 5535−5549

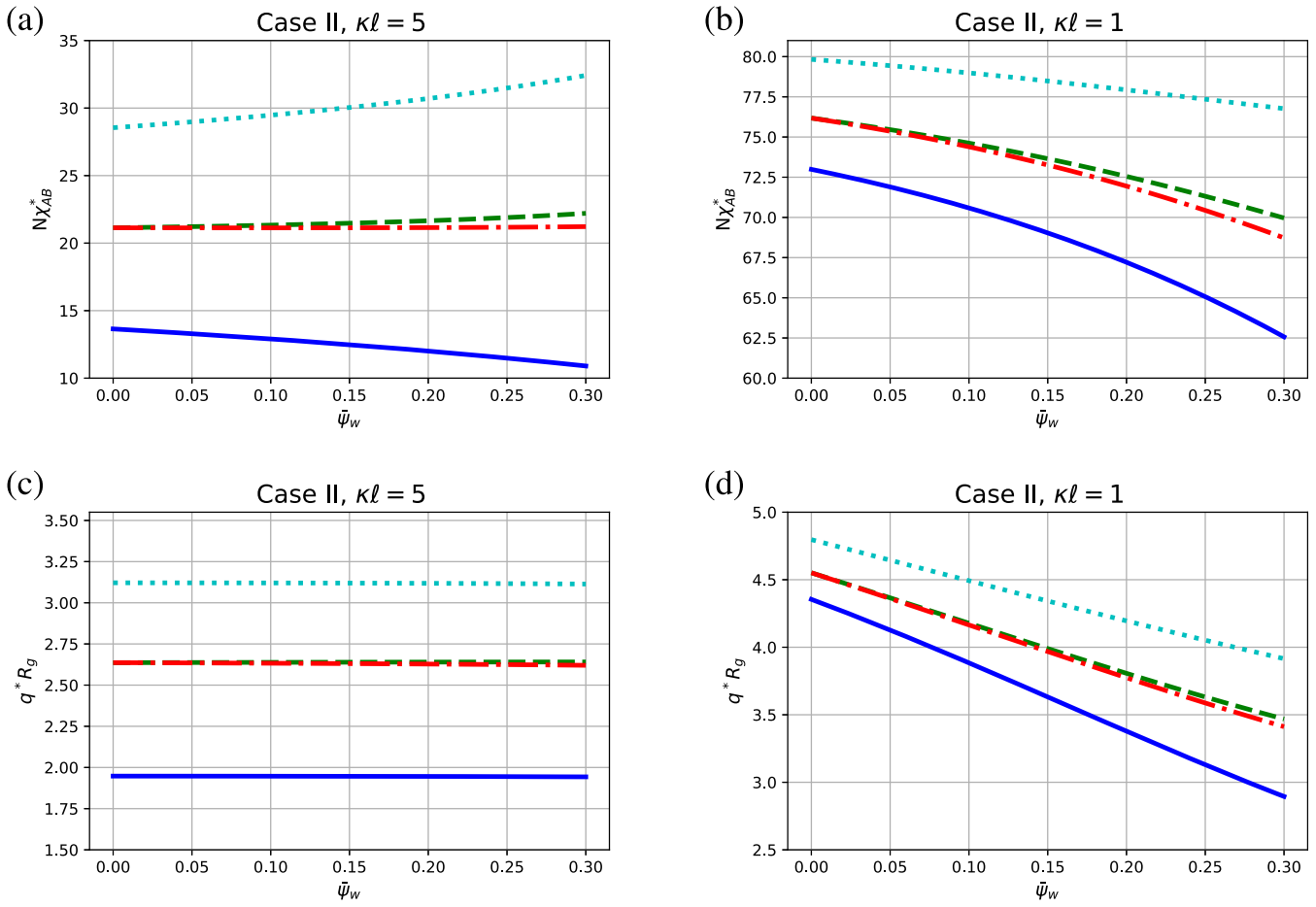

Figure 3. Same as Figure 2 for Case II.

correspond, respectively, to 92 mM and 2.3 M monovalent salt concentration. The latter salt concentration is close to the neutral limit.

Even in the disordered phase without any potential interactions or presence of solvent ($\chi_{AB} = 0$, $\bar{\psi}_w = 0$), the sequence plays a significant role in the formation of the microstructure. As an example, the normalized structure factor $G^{(2)}_{AA}(q)/N$ is given in Figure 1a as a function of qR_g (where $R_g = \sqrt{N/6}l$ is the radius of gyration of a Gaussian chain). A structure peak at an intermediate scattering wavevector q^* is evident for each of the sequences. For the diblock case (Seq 1), $q^*R_g = 1.85$, whereas for the alternating blocks of 50 monomers each (Seq 2), $q^*R_g = 3.0$. Therefore, smaller microstructures are selected by reducing the sequence order parameter. For Seq 3 and Seq 4, η is intermediate between Seq 1 and Seq 2, and hence $q^*R_g = 2.3$ is intermediate between the values for Seq 1 and Seq 2. The structure factors for Seq 3 and Seq 4 are identical owing to the fact that their structure factors are negative of each other in accordance with the Babinet principle.[57] The spinodal points at which the structure factor diverges at the scattering wavevector q^* are given below for the two cases of $\Delta\chi$. In addition, the $G^{(2)}_{AA}(q)/N$ of Seq 1 for Case II is given in Figure 1b. It shows a transition of peak q^* from a nonzero value to zero with an increasing amount of solvent. The interference between macro- and microstructures occurs around $\bar{\psi}_w = 0.95$, which is far from $\bar{\psi}_w = 0.0-0.3$, which we applied for spinodal points of microphase separation.

3.2.1. Case I (θ Solvent). For $\Delta\chi = 0$, the dependencies of $N\chi^*_{AB}$ and q^*R_g on the sequences are given in Figure 2 as functions of the solvent volume fraction $\bar{\psi}_w$. Both $N\chi^*_{AB}$ and q^*R_g depend crucially on the sequence. In general, a small η corresponds to a small sequence scale, and it implies that the confinements of conformations are strong when the microphase separation happens. As a result, $N\chi^*_{AB}$ increases with a reduction in the sequence order parameter η. As an example, Figures 2a and 2b show that $N\chi^*_{AB}$ increases in the order of Seqs 1, 4, 3, and 2. Also, for the present Case I, $N\chi^*_{AB}$ increases with the presence of solvent. Although the structure factor is identical for Seq 3 and Seq 4 in the absence of interactions and solvent, $N\chi^*_{AB}$ of Seq 3 is slightly higher than that for Seq 4 in the presence of the solvent. As seen in Figures 2a and 2b, $N\chi^*_{AB}$ increases by more than a factor of 2 upon a decrease in κl from 5 to 1 (equivalently from 2.3 M to 92 mM monovalent salt). The electrostatic repulsion between B segments is less screened at lower values of κl so that the disordered phase is more stable at lower salt concentrations as reflected in Figures 2a and 2b.

As shown in Figures 2c and 2d, the scattering wavevector q^* at the scattering peak depends on the sequence, and it increases in the order of Seq 1, 4, 3, and 2, analogous to the results in Figure 1. As the sequence order parameter η decreases, the spontaneously selected size of the microstructure decreases. As a result, q^* increases with a decrease in η. This feature, in conjunction with an increase in $N\chi^*_{AB}$, implies that microstructures of different sizes have different relative stabilities. It would be of future interest to investigate

https://doi.org/10.1021/acs.macromol.2c00008
Macromolecules 2022, 55, 5535−5549

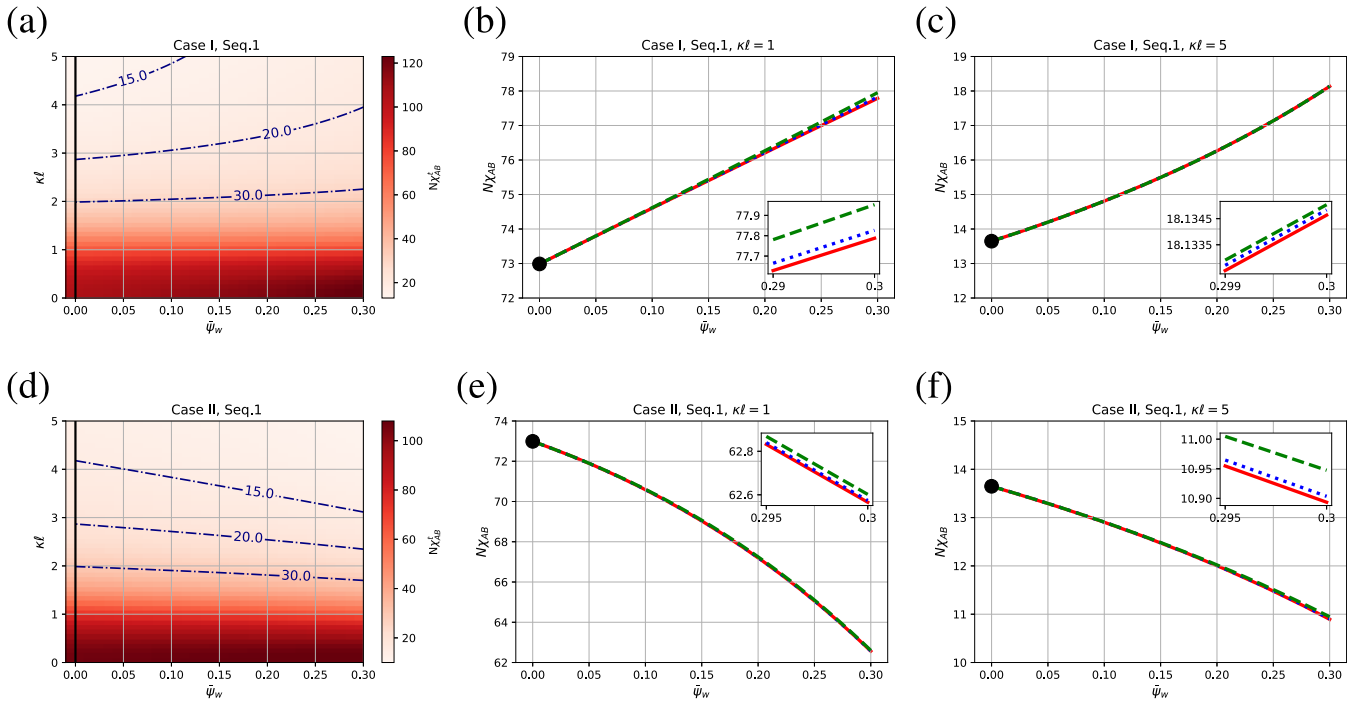

Figure 4. Morphology phase diagrams and transition points $N\chi^t_{AB}$ of Seq 1 for Cases I and II. (a) and (d) Heat maps of $N\chi^t_{AB}$; the black solid lines correspond to critical points. (b), (c), (e), and (f) Morphology phase diagrams for the two Cases at κl = 1 and 5: disorder−BCC (red solid, —), BCC−Hex (blue dotted, ···), and Hex−L (green dashed, ---); the black dots are critical points. The inset plots show tiny gaps among OOTs.

the free energy landscape as a function of the size of microstructures. As seen in Figures 2c and 2d, if the salt concentration is decreased, q^* increases for every sequence. Earlier work on uncharged−charged diblock copolymers shows that q^* increases with a decrease in κ.[40] An analogous result is evident in Figures 2c and 2d. It is of further interest to evaluate relative contributions from the translational entropy of small ions and excluded-volume and electrostatic interactions that are responsible for the behavior in Figures 2c and 2d.

3.2.2. Case II (Selective Solvent). When the solvent selectivity swells in B domains ($\Delta\chi$ = 0.2, χ_{Bw} = 0.3, and χ_{Aw} = 0.7) compared to A domains, the dependencies of $N\chi^*_{AB}$ and q^*R_g on the sequence and $\bar{\psi}_w$ are given in Figure 3. The increase in $N\chi^*_{AB}$ and q^*R_g with a decrease in κl is analogous to the results for Case I (Figure 2). Similarly, the dependence of q^*R_g on the solvent volume fraction $\bar{\psi}_w$ is qualitatively the same for both Case I and Case II. However, $N\chi^*_{AB}$ decreases with an increase in $\bar{\psi}_w$ in Case II, whereas the opposite trend is seen in Case I. This difference arises solely from the solvent selectivity in Case II. The magnitude of depression in $N\chi^*_{AB}$ due to $\bar{\psi}_w$ is smaller at higher values of κl (Figure 3a). Furthermore, Seq 1 and Seq 2 show the strongest opposite trends in Figure 3a. This trend can be qualitatively attributed to additional loop formation in the water-loving B domains, which are disfavored due to entropy.

3.3. Morphology Phase Diagrams. The spinodal points are not the exact points of the DOT because they only account for the instability, and hence $\Gamma^{(3)}_g$ and $\Gamma^{(4)}_g$ in F_g should be incorporated. By assuming that the fluctuations of density fields are dominated by the momentum at the spinodal points q^*,[39] the dominant density fields are

$$\Psi_g(\vec{r}) = \frac{\varphi}{\sqrt{n_m}} \sum_{k=1}^{n_m} [e^{i(\vec{Q}_k\cdot\vec{r}+\theta_k)} + e^{-i(\vec{Q}_k\cdot\vec{r}+\theta_k)}] \tag{65}$$

where $\vec{Q}_k$ are the reciprocal vectors corresponding to specific morphology, where $|\vec{Q}_k|$ is q^*. n_m is the number of distinct $\vec{Q}_k$, φ is the amplitude, and θ_k is the phase of $\vec{Q}_k$. For simplification, we only consider three conventional structures, namely, lamellar (L), hexagonal (Hex), and body-centered-cubic (BCC).[55] The information about $\vec{Q}_k$ and n_s of these structures and the details of the calculation are listed in the Supporting Information. Based on the above assumptions and structures, F_g is given by

$$\frac{NF_g}{\Omega k_B T} = N\lambda_g\varphi^2 + \beta_m\varphi^3 + \gamma_m\varphi^4 \tag{66}$$

where β_m (m = L, Hex, BCC) and γ_m are given below, and the corresponding minimum with respect to φ (keeping q^* fixed) is

$$\min\left\{\frac{(3|\beta_m| + \sqrt{9\beta_m^2 - 32N\lambda_g\gamma_m})^3(|\beta_m| - \sqrt{9\beta_m^2 - 32N\lambda_g\gamma_m})}{2^{12}\gamma_m^3}, 0\right\} \tag{67}$$

The β_m and γ_m for the three morphologies are

https://doi.org/10.1021/acs.macromol.2c00008
Macromolecules 2022, 55, 5535−5549

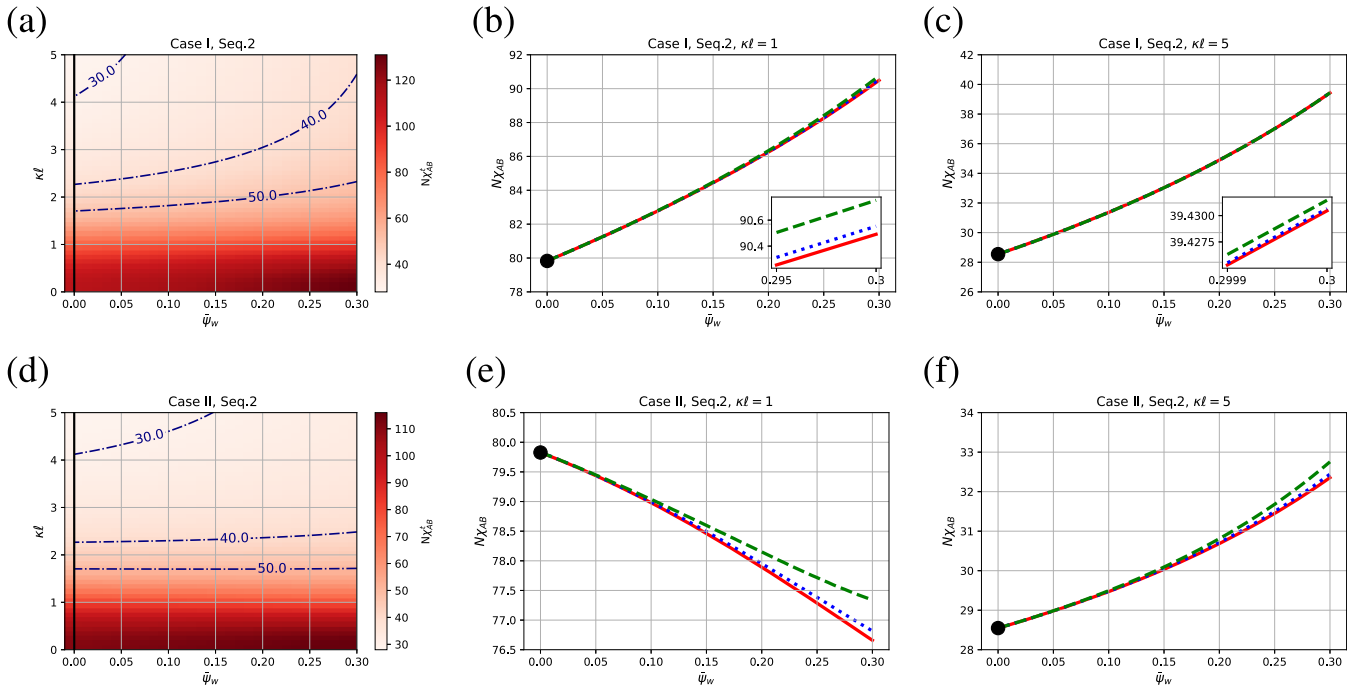

Figure 5. Same as Figure 4 for Seq 2.

$$\beta_{\mathrm{L}} = 0, \qquad \gamma_{\mathrm{L}} = N\frac{\Gamma_{\mathrm{g}}^{(4)}(0,0)}{4}$$

$$\beta_{\mathrm{Hex}} = \frac{2}{3\sqrt{3}}N\Gamma_{\mathrm{g}}^{(3)}(1), \qquad \gamma_{\mathrm{Hex}} = N\frac{\Gamma_{\mathrm{g}}^{(4)}(0,0) + \Gamma_{\mathrm{g}}^{(4)}(0,1)}{12}$$

$$\beta_{\mathrm{BCC}} = \frac{4}{3\sqrt{6}}N\Gamma_{\mathrm{g}}^{(3)}(1), \quad \gamma_{\mathrm{BCC}} = N\frac{\Gamma_{\mathrm{g}}^{(4)}(0,0) + 8\Gamma_{\mathrm{g}}^{(4)}(0,1) + 2\Gamma_{\mathrm{g}}^{(4)}(0,2) + 4\Gamma_{\mathrm{g}}^{(4)}(1,2)}{24} \tag{68}$$

where $\Gamma^{(3)}(\vec{q}_1, \vec{q}_2, \vec{q}_3)$ and $\Gamma^{(4)}(\vec{q}_1, \vec{q}_2, \vec{q}_3, \vec{q}_4)$ are reduced to $\Gamma^{(3)}(t)$, with $t \equiv |\vec{q}_1 + \vec{q}_2|^2/q^{*2}$, and $\Gamma^4(t_1, t_2)$, with $t_1 \equiv |\vec{q}_1 + \vec{q}_2|^2/q^{*2}$ and $t_2 \equiv |\vec{q}_1 + \vec{q}_4|^2/q^{*2}$, respectively (because the values of Γ are only dependent on the relative angles among vectors $\vec{q}$). It is to be noted that the mapping relation in eq 64 is modified by the solvent contribution in $N\Gamma_{\mathrm{g}}^{(3)}$ and $N\Gamma_{\mathrm{g}}^{(4)}$, namely, $N/\overline{\psi}_{\mathrm{w}}^2$ and $2N/\overline{\psi}_{\mathrm{w}}^3$ in eq 50 and eq 51.

First, the DOT occurs if the minimum value of eq 66 is smaller than 0. The corresponding points are denoted as χ_{AB}^t, which can be smaller than χ_{AB}^* because of the nonzero β. After DOT, the dominant structures of microphase separation are decided by the minimum value of eq 66 among these structures. These calculations of order−order transitions (OOTs) and DOT constitute the morphology phase diagrams for each sequence given in Figures 4−7. In the morphology diagrams, the order of transitions is always disorder−BCC−Hex−L. However, there are some critical points where the transition jumps from the disordered state to the L structure without going through BCC and Hex structures. The criterion of critical points is

$$\chi_{\mathrm{AB}}^t = \chi_{\mathrm{AB}}^* \tag{69}$$

which occurs if and only if

$$\beta_{\mathrm{L}} = \beta_{\mathrm{Hex}} = \beta_{\mathrm{BCC}} = N\Gamma_{\mathrm{g}}^{(3)}(1) = 0 \text{ at } (q^*, \chi_{\mathrm{AB}}^*) \tag{70}$$

The calculated heat maps of $N\chi_{\mathrm{AB}}^t$ with respect to $\overline{\psi}_{\mathrm{w}}$ and κl are plotted in Figures 4−7 for Case I and II for the four sequences. In addition, morphology phase diagrams with transitions among BCC, Hex, and L are given for $\kappa l = 1$ and 5. In the example of the heat map given in Figure 4a, the system represents Case I with Seq 1. As a guide to read the heat map, we have provided three curves ($N\chi_{\mathrm{AB}}^t$ = 30.0, 20.0, and 15.0) which portray the typical dependence of $N\chi_{\mathrm{AB}}^t$ on κl and $\overline{\psi}_{\mathrm{w}}$.

The heat maps of each sequence in both cases show that the χ_{AB}^t decreases as κl increases, and it implies that the repulsive electrostatic interactions among B monomers promote the disordered state. Whether χ_{AB}^t increases or decreases with $\overline{\psi}_{\mathrm{w}}$ depends on κl, the sequence, and Case I or II. The interplay among solvent quality, salt concentration, and sequences decides the properties of the microphase separations.

There are critical points as defined in eq 68 that appear in the heat maps and the morphology diagrams. They are denoted as solid black lines or black points. For Seq 1 and Seq 2, there are trivial critical points at $\overline{\psi}_{\mathrm{w}} = 0$ due to the Z_2 symmetry between A and B in each sequence. However, the morphology diagrams show that the gaps among OOTs are tiny. For Seq 3, there are no critical points because $\Gamma_{\mathrm{g}}^{(3)} \neq 0$. However, the difference between the spinodal points and the

https://doi.org/10.1021/acs.macromol.2c00008
Macromolecules 2022, 55, 5535−5549

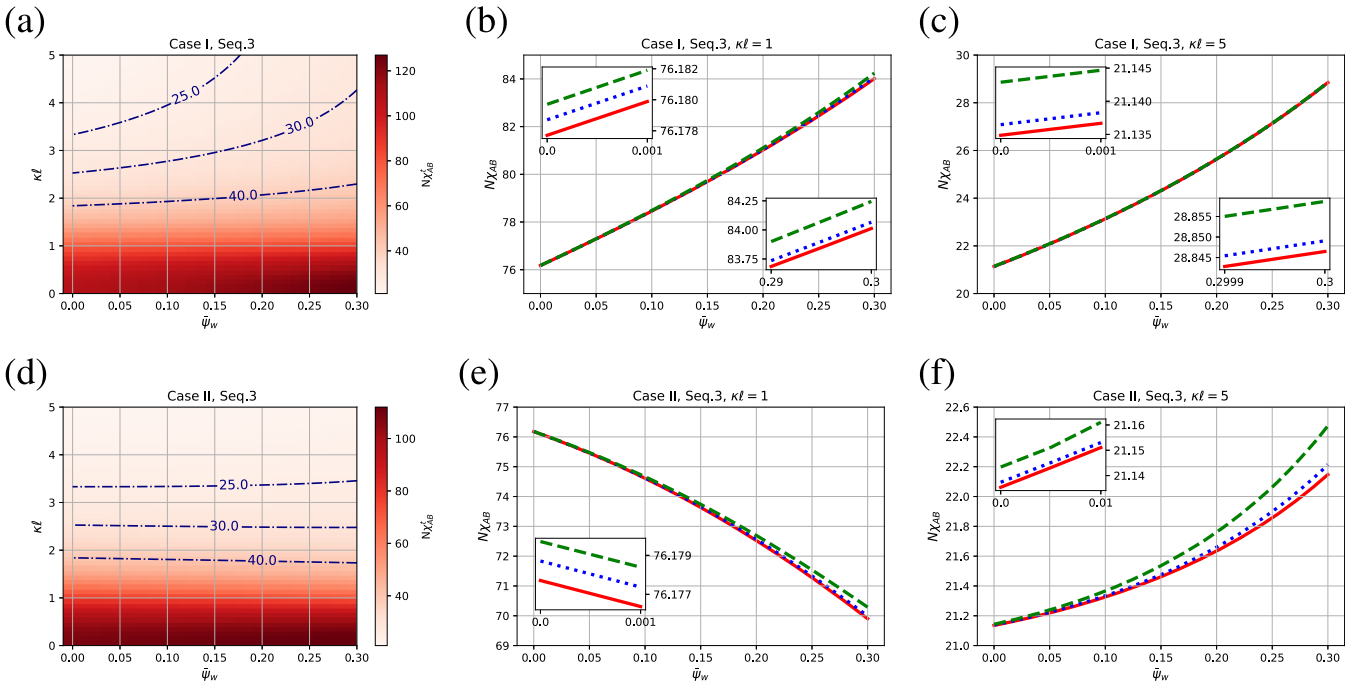

Figure 6. Same as Figure 4 for Seq 3, except that there are no critical points.

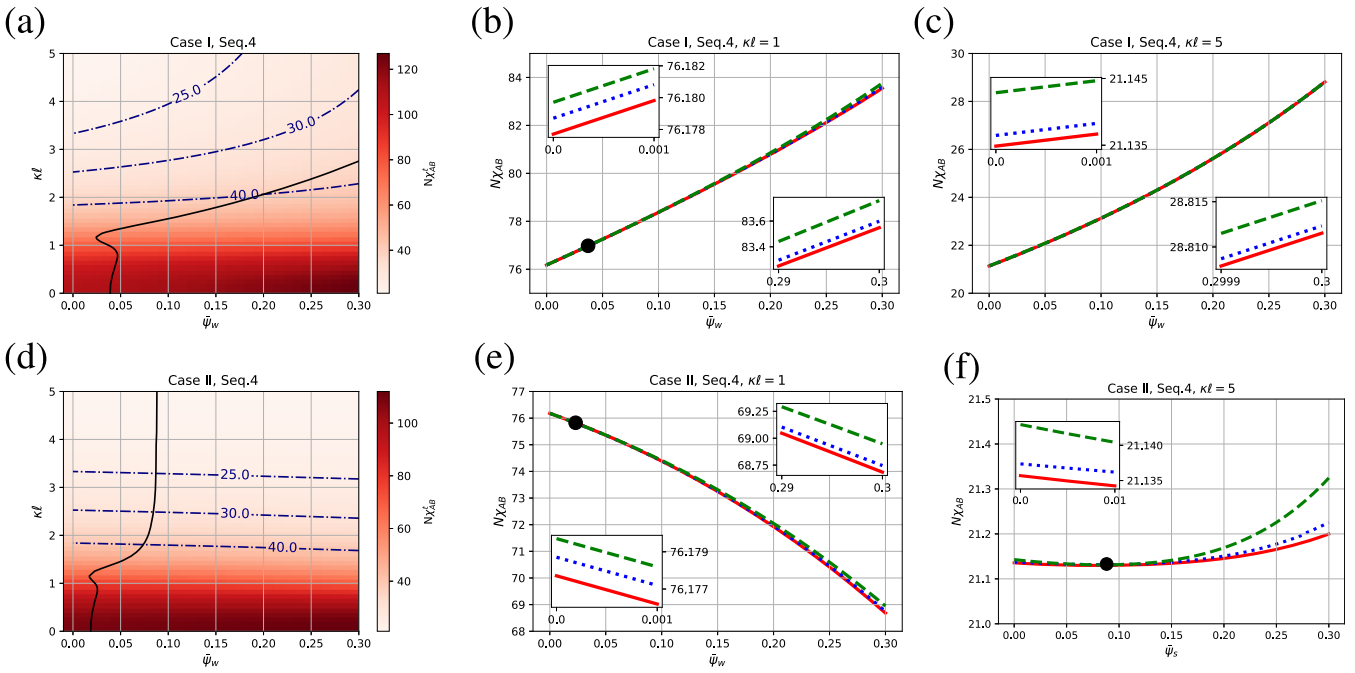

Figure 7. Same as Figure 4 for Seq 4.

DOT points is very small as exemplified in Figure 6c. In contrast, Seq 4 shows nontrivial curvy critical lines for both Cases I and II, as shown in Figure 7. These critical points disappear in Case I at high κl. However, they are present for Case II even at high κl.

4. CONCLUSIONS

Using a field-theoretic formalism, we have derived a general theory of microphase separation in a multicomponent solution of charged heteropolymers with specified sequences and small ions and solvent. The theory is pertinent to any thermodynamic system with an arbitrary number of components and an arbitrary number of different kinds of monomers constituting the heteropolymers with prescribed sequences. Based on the saddle point approximation, explicit formulas for the Helmholtz free energy are derived in the Landau−Ginzburg−Brazovskii form and the self-consistent field theory form in terms of polymer sequences and the various components in the system. We illustrate the implementation of this general theory by choosing a simple system made of a two-component heteropolymer with equal composition of neutral A monomers and charged B monomers and a salty solution and choosing four different sequences for the heteropolymer. For this illustrative example, we have calculated the structure factor in

https://doi.org/10.1021/acs.macromol.2c00008
Macromolecules 2022, 55, 5535−5549

the disordered phase, the stability limit of the disordered state, and the locations of the disorder−order transition and order−order transitions with the three canonical examples of the ordered phase, namely BCC, hexagonal, and lamellar morphologies.

Even for the simple illustrative example demonstrated here, we find that the polymer sequences play a profound role in the spontaneous selection of microstructures and the onset of microphase separation and the quantitative nature of the various order−order transitions among different morphological structures. To be specific, we have studied the scattering peak q^* in the disordered phase, spinodal point $N\chi^*_{AB}$, and the transition points $N\chi^t_{AB}$ for the four sequences $A_{50}A_{50}B_{50}B_{50}$, $A_{50}B_{50}A_{50}B_{50}$, $A_{50}B_{50}B_{50}A_{50}$, and $B_{50}A_{50}A_{50}B_{50}$, where $N = 200$ and χ_{AB} is the Flory−Huggins parameter for the A and B monomers (A is neutral and B is charged). Defining a sequence order parameter η as the reciprocal of the number of domain walls separating adjacent A and B blocks, we find (a) the size of the spontaneously selected microstructure for A domains increases with an increase in η and salt concentration, and (b) $N\chi^*_{AB}$ increases with a decrease in η and salt concentration. We also find that the solvent quality is an important contributor to the dependence of $N\chi^*_{AB}$ on η and salt concentration. While $N\chi^*_{AB}$ increases with the volume fraction of the solvent for mutual theta solvents for both A and B, the opposite trend is predicted for a selective solvent for B. While the qualitative features of the predicted morphology diagrams track the above results of $N\chi^*_{AB}$ for Seq 1 and Seq 2, the morphology phase diagram become much richer for Seq 3 and Seq 4.

The present work provides a computational engine to address microphase separation in complex multicomponent systems including the solutions of intrinsically disordered proteins. Even though the illustration of the rich sequence effects on microphase separation is presented here in the weak segregation limit, the formulas provided here allow consideration of the strong segregation limit as well. The implementation of the present general theory for specific sequences of experimental and biological interests is relegated to future work.

■ ASSOCIATED CONTENT

Supporting Information

The Supporting Information is available free of charge at https://pubs.acs.org/doi/10.1021/acs.macromol.2c00008.

Derivations of the self-consistent field theory, the general theory, evaluations of correlations, eq 58, and values of β and γ (PDF)

■ AUTHOR INFORMATION

Corresponding Author

Murugappan Muthukumar − *Department of Polymer Science and Engineering, University of Massachusetts, Amherst, Massachusetts 01003, United States;* orcid.org/0000-0001-7872-4883; Email: muthu@polysci.umass.edu

Author

Siao-Fong Li − *Department of Physics, University of Massachusetts, Amherst, Massachusetts 01003, United States*

Complete contact information is available at: https://pubs.acs.org/10.1021/acs.macromol.2c00008

Notes

The authors declare no competing financial interest.

■ ACKNOWLEDGMENTS

This research was supported by the AFOSR (Grant No. FA 9550-20-1-0142) and the National Science Foundation (Grant No. DMR-2015935).

■ REFERENCES

(1) Dinic, J.; Marciel, A. B.; Tirrell, M. V. Polyampholyte physics: Liquid-liquid phase separation and biological condensates. *Curr. Opin. Colloid Interface Sci.* **2021**, *54*, 101457.

(2) Nam, K. T.; Shelby, S. A.; Choi, P. H.; Marciel, A. B.; Chen, R.; Tan, L.; Chu, T. K.; Mesch, R. A.; Lee, B.-C.; Connolly, M. D.; Kisielowski, C.; Zuckermann, R. N.; et al. Free-floating ultrathin two-dimensional crystals from sequence-specific peptoid polymers. *Nat. Mater.* **2010**, *9*, 454−460.

(3) Rosales, A. M.; Segalman, R. A.; Zuckermann, R. N. Polypeptoids: a model system to study the effect of monomer sequence on polymer properties and self-assembly. *Soft Matter* **2013**, *9*, 8400−8414.

(4) Anfinsen, C. B. Principles that govern the folding of protein chains. *Science* **1973**, *181*, 223−230.

(5) Sawle, L.; Ghosh, K. A theoretical method to compute sequence dependent configurational properties in charged polymers and proteins. *J. Chem. Phys.* **2015**, *143*, 085101.

(6) Firman, T.; Ghosh, K. Sequence charge decoration dictates coil-globule transition in intrinsically disordered proteins. *J. Chem. Phys.* **2018**, *148*, 123305.

(7) Huihui, J.; Firman, T.; Ghosh, K. Modulating charge patterning and ionic strength as a strategy to induce conformational changes in intrinsically disordered proteins. *J. Chem. Phys.* **2018**, *149*, 085101.

(8) Huihui, J.; Ghosh, K. An analytical theory to describe sequence-specific inter-residue distance profiles for polyampholytes and intrinsically disordered proteins. *J. Chem. Phys.* **2020**, *152*, 161102.

(9) Das, R. K.; Pappu, R. V. Conformations of intrinsically disordered proteins are influenced by linear sequence distributions of oppositely charged residues. *Proc. Natl. Acad. Sci. U.S.A.* **2013**, *110*, 13392−13397.

(10) Martin, E. W.; Holehouse, A. S.; Grace, C. R.; Hughes, A.; Pappu, R. V.; Mittag, T. Sequence determinants of the conformational properties of an intrinsically disordered protein prior to and upon multisite phosphorylation. *J. Am. Chem. Soc.* **2016**, *138*, 15323−15335.

(11) Mittal, A.; Holehouse, A. S.; Cohan, M. C.; Pappu, R. V. Sequence-to-conformation relationships of disordered regions tethered to folded domains of proteins. *J. Mol. Biol.* **2018**, *430*, 2403−2421.

(12) Perutz, M. Electrostatic effects in proteins. *Science* **1978**, *201*, 1187−1191.

(13) Helfand, E. Theory of inhomogeneous polymers: Fundamentals of the Gaussian random-walk model. *J. Chem. Phys.* **1975**, *62*, 999−1005.

(14) Helfand, E. Block copolymer theory. III. Statistical mechanics of the microdomain structure. *Macromolecules* **1975**, *8*, 552−556.

(15) Helfand, E.; Wasserman, Z. Block copolymer theory. 5. Spherical domains. *Macromolecules* **1978**, *11*, 960−966.

(16) Helfand, E.; Wasserman, Z.; Weber, T. A. Brownian Dynamics Study of Polymer Conformational Transitions±. *Macromolecules* **1980**, *13*, 526−533.

(17) Semenov, A. Microphase separation in diblock-copolymer melts: ordering of micelles. *Macromolecules* **1989**, *22*, 2849−2851.

(18) Ohta, T.; Kawasaki, K. Equilibrium morphology of block copolymer melts. *Macromolecules* **1986**, *19*, 2621−2632.

(19) Kawasaki, K.; Ohta, T.; Kohrogui, M. Equilibrium morphology of block copolymer melts. 2. *Macromolecules* **1988**, *21*, 2972−2980.

(20) Kawasaki, K.; Kawakatsu, T. Equilibrium morphology of block copolymer melts. 3. *Macromolecules* **1990**, *23*, 4006−4019.

(21) Matsen, M. W.; Schick, M. Stable and unstable phases of a diblock copolymer melt. *Phys. Rev. Lett.* **1994**, *72*, 2660−2663.
(22) Matsen, M. W.; Bates, F. S. Unifying weak-and strong-segregation block copolymer theories. *Macromolecules* **1996**, *29*, 1091−1098.
(23) Matsen, M. W. The standard Gaussian model for block copolymer melts. *J. Phys.: Condens. Matter* **2002**, *14*, R21.
(24) Fredrickson, G. H.; Helfand, E. Fluctuation effects in the theory of microphase separation in block copolymers. *J. Chem. Phys.* **1987**, *87*, 697−705.
(25) Olvera de La Cruz, M. Transitions to periodic structures in block copolymer melts. *Phys. Rev. Lett.* **1991**, *67*, 85−88.
(26) Shi, A.-C.; Noolandi, J. Theory of inhomogeneous weakly charged polyelectrolytes. *Macromol. Theory Simul.* **1999**, *8*, 214−229.
(27) Lewis, R. M., III; Arora, A.; Beech, H. K.; Lee, B.; Lindsay, A. P.; Lodge, T. P.; Dorfman, K. D.; Bates, F. S. Role of chain length in the formation of Frank-Kasper phases in diblock copolymers. *Phys. Rev. Lett.* **2018**, *121*, 208002.
(28) Arora, A.; Pillai, N.; Bates, F. S.; Dorfman, K. D. Predicting the phase behavior of ABAC tetrablock terpolymers: Sensitivity to Flory-Huggins interaction parameters. *Polymer* **2018**, *154*, 305−314.
(29) Bohbot-Raviv, Y.; Wang, Z.-G. Discovering new ordered phases of block copolymers. *Phys. Rev. Lett.* **2000**, *85*, 3428.
(30) Zheng, W.; Wang, Z.-G. Morphology of ABC triblock copolymers. *Macromolecules* **1995**, *28*, 7215−7223.
(31) Smirnova, Y. G.; ten Brinke, G.; Erukhimovich, I. Y. Microphase separation in multiblock copolymer melts: Nonconventional morphologies and two-length-scale switching. *J. Chem. Phys.* **2006**, *124*, 054907.
(32) Nap, R.; Sushko, N.; Erukhimovich, I.; Ten Brinke, G. Double periodic lamellar-in-lamellar structure in multiblock copolymer melts with competing length scales. *Macromolecules* **2006**, *39*, 6765−6770.
(33) Sing, C. E.; Zwanikken, J. W.; De La Cruz, M. O. Electrostatic control of block copolymer morphology. *Nat. Mater.* **2014**, *13*, 694−698.
(34) Xie, J.; Shi, A.-C. Formation of complex spherical packing phases in diblock copolymer/homopolymer blends. *Giant* **2021**, *5*, 100043.
(35) Jiang, J.; Chen, X.; Yang, S.; Chen, E.-Q. The size and affinity effect of counterions on self-assembly of charged block copolymers. *J. Chem. Phys.* **2020**, *152*, 124901.
(36) Rabin, Y.; Marko, J. Microphase separation in charged diblock copolymers: the weak segregation limit. *Macromolecules* **1991**, *24*, 2134−2136.
(37) Marko, J.; Rabin, Y. Microphase separation of charged diblock copolymers: melts and solutions. *Macromolecules* **1992**, *25*, 1503−1509.
(38) Muthukumar, M. Fluctuation effects in the density functional theory of order-disorder transitions in block copolymers. *Macromolecules* **1993**, *26*, 5259−5261.
(39) Leibler, L. Theory of microphase separation in block copolymers. *Macromolecules* **1980**, *13*, 1602−1617.
(40) Kumar, R.; Muthukumar, M. Microphase separation in polyelectrolytic diblock copolymer melt: weak segregation limit. *J. Chem. Phys.* **2007**, *126*, 214902.
(41) Perry, S. L.; Sing, C. E. 100th anniversary of macromolecular science viewpoint: Opportunities in the physics of sequence-defined polymers. *ACS Macro Lett.* **2020**, *9*, 216−225.
(42) Patterson, A. L.; Danielsen, S. P.; Yu, B.; Davidson, E. C.; Fredrickson, G. H.; Segalman, R. A. Sequence effects on block copolymer self-assembly through tuning chain conformation and segregation strength utilizing sequence-defined polypeptoids. *Macromolecules* **2019**, *52*, 1277−1286.
(43) Srivastava, D.; Muthukumar, M. Sequence dependence of conformations of polyampholytes. *Macromolecules* **1996**, *29*, 2324−2326.
(44) Khokhlov, A. R.; Khalatur, P. G. Conformation-dependent sequence design (engineering) of AB copolymers. *Physical review letters* **1999**, *82*, 3456.
(45) Govorun, E. N.; Ivanov, V. A.; Khokhlov, A. R.; Khalatur, P. G.; Borovinsky, A. L.; Grosberg, A. Y. Primary sequences of proteinlike copolymers: Levy-flight-type long-range correlations. *Phys. Rev. E* **2001**, *64*, 040903.
(46) Kielhorn, L.; Muthukumar, M. Fluctuation theory of diblock copolymer/homopolymer blends and its effects on the Lifshitz point. *J. Chem. Phys.* **1997**, *107*, 5588−5608.
(47) Muthukumar, M. Double screening in polyelectrolyte solutions: Limiting laws and crossover formulas. *J. Chem. Phys.* **1996**, *105*, 5183−5199.
(48) Muthukumar, M. Phase diagram of polyelectrolyte solutions: weak polymer effect. *Macromolecules* **2002**, *35*, 9142−9145.
(49) Muthukumar, M. Electrostatic correlations in polyelectrolyte solutions. *Polymer Science Series A* **2016**, *58*, 852−863.
(50) Muthukumar, M. 50th anniversary perspective: A perspective on polyelectrolyte solutions. *Macromolecules* **2017**, *50*, 9528−9560.
(51) Shen, K.; Wang, Z.-G. Electrostatic correlations and the polyelectrolyte self energy. *J. Chem. Phys.* **2017**, *146*, 084901.
(52) Liu, Y.-X.; Zhang, H.-D.; Tong, C.-H.; Yang, Y.-L. Microphase separation and phase diagram of concentrated diblock copolyelectrolyte solutions studied by self-consistent field theory calculations in two-dimensional space. *Macromolecules* **2011**, *44*, 8261−8269.
(53) McQuarrie, D. A. *Statistical Mechanics*; University Science Books: Sausalito, CA, 2000.
(54) Schwartz, M. D. *Quantum Field Theory and the Standard Model*; Cambridge University Press: Cambridge, U.K., 2014.
(55) Erukhimovich, I. Y. Weak segregation theory and non-conventional morphologies in the ternary ABC triblock copolymers. *Eur. Phys. J. E Soft Matter* **2005**, *18*, 383−406.
(56) de Gennes, P.-G. *Scaling Concepts in Polymer Physics*; Cornell University Press: Ithaca, NY, 1979.
(57) Higgins, J. S.; Benoit, H. C. *Polymers and Neutron Scattering*; Clarendon Press: Oxford, U.K., 1994.

https://doi.org/10.1021/acs.macromol.2c00008
Macromolecules 2022, 55, 5535−5549